

Probing new physics with $\bar{B} \rightarrow \rho(770)\ell^-\bar{\nu}_\ell$ and $\bar{B} \rightarrow a_1(1260)\ell^-\bar{\nu}_\ell$

P. Colangelo¹, F. De Fazio¹, and F. Loporco^{2,1}

¹*Istituto Nazionale di Fisica Nucleare, Sezione di Bari, via Orabona 4, 70126 Bari, Italy*

²*Dipartimento Interateneo di Fisica “Michelangelo Merlin”, Università degli Studi di Bari, via Orabona 4, 70126 Bari, Italy*



(Received 20 August 2019; published 31 October 2019)

The B meson semileptonic modes to $\rho(770)$ and $a_1(1260)$ are useful to pin down possible non-Standard Model effects. The four-dimensional differential $\bar{B} \rightarrow \rho(\pi\pi)\ell^-\bar{\nu}_\ell$ and $\bar{B} \rightarrow a_1(\rho\pi)\ell^-\bar{\nu}_\ell$ decay distributions are computed in the Standard Model and in extensions involving new lepton-flavor universality violating semileptonic $b \rightarrow u$ operators. The large energy limit for the light meson is also considered for both modes. The new effective couplings are constrained using the available data, and several observables in $\bar{B} \rightarrow \rho(\pi\pi)\ell^-\bar{\nu}_\ell$ in which new physics effects can be better identified are selected, using the angular coefficient functions. The complementary role of $\bar{B} \rightarrow \rho(\pi\pi)\ell^-\bar{\nu}_\ell$ and $\bar{B} \rightarrow a_1(\rho\pi)\ell^-\bar{\nu}_\ell$ is discussed.

DOI: 10.1103/PhysRevD.100.075037

I. INTRODUCTION

The anomalies that recently emerged in the flavor sector challenge both the experimental analyses and the theoretical interpretations. In the tree-level $b \rightarrow c\ell^-\bar{\nu}_\ell$ process, deviations of the ratios $R(D^{(*)}) = \frac{\mathcal{B}(B \rightarrow D^{(*)}\tau^-\bar{\nu}_\tau)}{\mathcal{B}(B \rightarrow D^{(*)}\ell^-\bar{\nu}_\ell)}$ (with $\ell = e, \mu$) from the Standard Model (SM) expectations have been observed by *BABAR* [1,2], *Belle* [3–6], and *LHCb* [7–9]. The measurements can be summarized as $R(D)_{\text{exp}} = 0.407 \pm 0.039 \pm 0.024$ to be combined with the new *Belle* result $R(D)_{\text{exp}} = 0.307 \pm 0.037 \pm 0.016$ [10], and $R(D^*)_{\text{exp}} = 0.295 \pm 0.011 \pm 0.008$. These measurements are 3.1σ away from the SM values quoted by the Heavy Flavor Averaging Group (HFLAG) [11]: $R(D)_{\text{SM}} = 0.299 \pm 0.003$ and $R(D^*)_{\text{SM}} = 0.258 \pm 0.005$. The tension, noticed in Ref. [12], is significant since the hadronic uncertainties largely cancel out in the ratios of branching fractions [13]. The *LHCb* measurement $R(J/\psi) = \frac{\mathcal{B}(B_c^+ \rightarrow J/\psi\tau^+\nu_\tau)}{\mathcal{B}(B_c^+ \rightarrow J/\psi\mu^+\nu_\mu)} = 0.71 \pm 0.17(\text{stat}) \pm 0.18(\text{syst})$ [14] also exceeds the SM expectation; however, in these modes, the hadronic uncertainties are sizable [15–17].

Other anomalies have been detected in neutral current $b \rightarrow s$ semileptonic transitions, in the ratios $R_{K^{(*)}} = \frac{\int_{q_{\text{min}}^2}^{q_{\text{max}}^2} \frac{d\Gamma}{dq^2}(B^+ \rightarrow K^{(*)}\mu^+\mu^-)dq^2}{\int_{q_{\text{min}}^2}^{q_{\text{max}}^2} \frac{d\Gamma}{dq^2}(B^+ \rightarrow K^{(*)}e^+e^-)dq^2}$ measured by *LHCb* and *Belle*.

The updated result for R_K is $R_{K^+} = 0.846_{-0.054}^{+0.060} \times (\text{stat})_{-0.014}^{-0.016}(\text{syst})$ for $[q_{\text{min}}^2, q_{\text{max}}^2] = [1.1 \text{ GeV}^2, 6 \text{ GeV}^2]$ [18]. For R_{K^*} , the measurements $R_{K^{*0}} = 0.66 \pm 0.11(\text{stat}) \pm 0.03(\text{syst})$ for q^2 in $[0.045 \text{ GeV}^2, 1.1 \text{ GeV}^2]$ and $R_{K^{*+}} = 0.69 \pm 0.11(\text{stat}) \pm 0.05(\text{syst})$ for q^2 in $[1.1 \text{ GeV}^2, 6 \text{ GeV}^2]$ have been reported by *LHCb* [19]. Recent *Belle* measurements, averaged over the neutral and charged modes, are affected by larger errors: $R_{K^*} = 0.52 \pm 0.36(\text{stat}) \pm 0.05(\text{syst})$ for q^2 in $[0.045 \text{ GeV}^2, 1.1 \text{ GeV}^2]$, $R_{K^*} = 0.90 \pm 0.27(\text{stat}) \pm 0.10(\text{syst})$ for q^2 in $[0.1 \text{ GeV}^2, 8 \text{ GeV}^2]$, and $R_{K^*} = 1.18 \pm 0.52(\text{stat}) \pm 0.10(\text{syst})$ for q^2 in $[15 \text{ GeV}^2, 19 \text{ GeV}^2]$ [20]. For all the ratios, the SM predictions are close to 1.

The anomalies in $b \rightarrow c$ and $b \rightarrow s$ semileptonic modes seem to point to violation of lepton-flavor universality (LFU). This accidental SM symmetry is only broken by the Yukawa interactions, while the lepton couplings to the gauge bosons are independent of the lepton flavor.¹ It is unclear if the deviations that emerged in angular observables in $B \rightarrow K^*\mu^+\mu^-$ [22,23] and in the rate of $B_s^0 \rightarrow \phi\mu^+\mu^-$ [24] can have a connected origin.

In addition to these tensions, the long-standing difference in the determination of the Cabibbo-Kobayashi-Maskawa (CKM) matrix element $|V_{cb}|$ from exclusive modes, in particular $\bar{B} \rightarrow D^*\ell^-\bar{\nu}_\ell$, and from inclusive $\bar{B} \rightarrow X_c\ell^-\bar{\nu}_\ell$ observables (width and moments) still persists in new *BABAR* [25] and *Belle* analyses [26], with $|V_{cb}|_{\text{excl}} < |V_{cb}|_{\text{incl}}$. As an alternative to solutions to the puzzle within the SM [27–30], a connection has been proposed with the other $b \rightarrow c$ anomalies, within a LFU violating framework [13,31]. The related

¹For a review on LFU tests, see Ref. [21].

Published by the American Physical Society under the terms of the [Creative Commons Attribution 4.0 International license](https://creativecommons.org/licenses/by/4.0/). Further distribution of this work must maintain attribution to the author(s) and the published article's title, journal citation, and DOI. Funded by SCOAP³.

experimental signatures have been studied, in particular, the four-dimensional differential $\bar{B} \rightarrow D^*(D\pi, D\gamma)\ell^-\bar{\nu}_\ell$ decay distributions for the three lepton species have been scrutinized [32], following analyses that have pointed out the relevance of such distributions [33–36].

It is worth wondering if similar deviations can appear in semileptonic $b \rightarrow u$ transitions. These modes are CKM suppressed with respect to the $b \rightarrow c$ ones; nevertheless, high precision measurements are foreseen in the near future by LHCb and Belle II. At present, there is a tension between the exclusive measurement of $|V_{ub}|$, mainly from the $\bar{B} \rightarrow \pi\ell^-\bar{\nu}_\ell$ decay width, and the inclusive determination from $\bar{B} \rightarrow X_u\ell^-\bar{\nu}_\ell$ observables. New information is available on the purely leptonic and on the semileptonic $B \rightarrow \pi$ mode, and analyses within and beyond SM have been carried out [37–45].

Other decay modes can be exploited to pin down deviation from the Standard Model. In particular, for the modes involving the vector $\rho(770)$ and the axial-vector $a_1(1260)$ mesons, the fully differential angular distributions when rho decays into two pions and a_1 decays into $\rho\pi$ represent an important source of information, due to the wealth of observables that can be analyzed. Such observables are all correlated and are able to provide coherent patterns within SM and its possible extensions. The different parities of the two mesons act as a filter for new physics (NP) operators, which is one of the prime motivations for their consideration. In addition, the $a_1 \rightarrow \rho\pi$ mode has the peculiarity that the longitudinal and transverse ρ polarizations are involved, increasing the plethora of observables on which to focus the experimental analyses. Our NP extension includes lepton-flavor dependent operators, and the comparison with the effects of corresponding $b \rightarrow c$ operators could shed light on the structure of the observed LFU violating effects.

In Sec. II, we introduce the semileptonic $b \rightarrow u$ effective Hamiltonian with the inclusion of new scalar, pseudoscalar, vector, and tensor operators weighted by complex couplings. Such operators affect the \bar{B} transitions to two leptons and to $\pi\ell\bar{\nu}$, and both channels can be exploited to bound the effective coefficients. In Sec. III, we construct the fully differential decay distributions for the $\bar{B} \rightarrow \rho(\pi\pi)\ell^-\bar{\nu}_\ell$ and $\bar{B} \rightarrow a_1(\rho\pi)\ell^-\bar{\nu}_\ell$ modes, computing the sets of angular coefficient functions in terms of the hadronic matrix elements involved in the transitions. We also consider the large energy limit for the light mesons, which allows us to express the angular functions in terms of a small number of hadronic form factors. In Sec. IV, we analyze several observables in $\bar{B} \rightarrow \rho(\pi\pi)\ell^-\bar{\nu}_\ell$ at a benchmark point in the parameter space of the new couplings, to scrutinize their sensitivity to the different new operators. In particular, we focus on the angular coefficient functions and on combinations for which the new operators would exhibit the largest effect. In Sec. V, we elaborate on the $a_1(1260)$ mode; in such a case, the uncertainties on the sets of hadronic form

factors are large and still need to be precisely assessed. Nevertheless, we present a numerical analysis of a few observables, to show the sensitivity of the a_1 mode to NP, but the main focus is on the analytic results and on the outcome of the large energy limit, to explain the complementarity with the ρ mode. The last section contains a discussion of the interesting perspectives and the conclusions. In the Appendixes, we collect the definitions of the hadronic matrix elements and the expressions of the angular coefficient functions for the two modes.

II. EFFECTIVE $b \rightarrow u\ell^-\bar{\nu}_\ell$ NP HAMILTONIAN AND IMPACT ON B MESON PURELY LEPTONIC AND SEMILEPTONIC PION MODES

New physics contributions to beauty hadron decays can be analyzed within the Standard Model Effective Field Theory. If the NP scale Λ_{NP} is much larger than the electroweak (EW) scale, all the new massive degrees of freedom can be integrated out, obtaining an effective Hamiltonian in which only the SM fields appear and which is invariant under the SM gauge group. This Hamiltonian contains additional operators with respect to the SM, suppressed by increasing powers of Λ_{NP} . The contribution $\mathcal{O}(\frac{1}{\Lambda_{\text{NP}}^2})$ includes dimension-6 four-fermion operators [46].

To describe the modes $\bar{B} \rightarrow M_u\ell^-\bar{\nu}_\ell$ with M_u a light meson comprising an up quark, we consider the effective Hamiltonian

$$H_{\text{eff}}^{b \rightarrow u\ell\nu} = \frac{G_F}{\sqrt{2}} V_{ub} \left\{ (1 + \epsilon_V^\ell)(\bar{u}\gamma_\mu(1 - \gamma_5)b)(\bar{\ell}\gamma^\mu(1 - \gamma_5)\nu_\ell) + \epsilon_S^\ell(\bar{u}b)(\bar{\ell}(1 - \gamma_5)\nu_\ell) + \epsilon_P^\ell(\bar{u}\gamma_5b)(\bar{\ell}(1 - \gamma_5)\nu_\ell) + \epsilon_T^\ell(\bar{u}\sigma_{\mu\nu}(1 - \gamma_5)b)(\bar{\ell}\sigma^{\mu\nu}(1 - \gamma_5)\nu_\ell) \right\} + \text{H.c.}, \quad (1)$$

consisting in the SM term and in NP terms weighted by complex lepton-flavor dependent couplings $\epsilon_{V,S,P,T}^\ell V_{ub}$ and ϵ_V^ℓ are independent parameters, since the product $V_{ub}(1 + \epsilon_V^\ell)$ is not a mere redefinition of the SM V_{ub} . We assume a purely left-handed lepton current as in the SM, an extensively probed structure. We exclude the quark right-handed vector current, since the only four-fermion operator of this type, invariant under the SM group, is nonlinear in the Higgs field [47–49].²

The couplings of the NP operators in (1) are constrained by the measurements, in particular on the purely leptonic B^- and semileptonic $\bar{B} \rightarrow \pi\ell^-\bar{\nu}_\ell$ channels. Indeed, the $B^- \rightarrow \ell^-\bar{\nu}_\ell$ decay width obtained from $H_{\text{eff}}^{b \rightarrow u\ell\nu}$ in Eq. (1) reads

²Right-handed currents are investigated in Refs. [38,39,41].

$$\Gamma(B^- \rightarrow \ell^- \bar{\nu}_\ell) = \frac{G_F^2 |V_{ub}|^2 f_B^2 m_B^3}{8\pi} \left(1 - \frac{m_\ell^2}{m_B^2}\right)^2 \left(\frac{m_\ell}{m_B}\right) \times \left(1 + \epsilon_V^\ell\right) + \frac{m_B}{m_b + m_u} \epsilon_P^\ell \Big|^2, \quad (2)$$

with the decay constant f_B defined as

$$\langle 0 | \bar{u} \gamma_\mu \gamma_5 b | \bar{B}(p) \rangle = i f_B p_\mu. \quad (3)$$

The EW correction to (2) is tiny. This mode is insensitive to the NP scalar and tensor operators. The pseudoscalar operator removes the helicity suppression, which is effective for light leptons, with a consequent stringent constraint for the effective couplings $\epsilon_P^{\ell,\mu}$.

The semileptonic $\bar{B} \rightarrow \pi \ell^- \bar{\nu}_\ell$ decay distribution in the dilepton mass squared q^2 , obtained from Eq. (1) parametrizing the weak matrix element in terms of the form factors $f_i(q^2) = f_i^{B \rightarrow \pi}(q^2)$ as in Appendix A, is

$$\begin{aligned} \frac{d\Gamma}{dq^2}(\bar{B} \rightarrow \pi \ell^- \bar{\nu}_\ell) &= \frac{G_F^2 |V_{ub}|^2 \lambda^{1/2}(m_B^2, m_\pi^2, q^2)}{128 m_B^3 \pi^3 q^2} \left(1 - \frac{m_\ell^2}{q^2}\right)^2 \\ &\times \left\{ \left| m_\ell (1 + \epsilon_V^\ell) + \frac{q^2 \epsilon_S^\ell}{m_b - m_u} \right|^2 (m_B^2 - m_\pi^2)^2 f_0^2(q^2) \right. \\ &+ \lambda(m_B^2, m_\pi^2, q^2) \left[\frac{1}{3} \left| m_\ell (1 + \epsilon_V^\ell) f_+(q^2) + \frac{4q^2}{m_B + m_\pi} \epsilon_T^\ell f_T(q^2) \right|^2 \right. \\ &\left. \left. + \frac{2q^2}{3} \left| (1 + \epsilon_V^\ell) f_+(q^2) + 4 \frac{m_\ell}{m_B + m_\pi} \epsilon_T^\ell f_T(q^2) \right|^2 \right] \right\}, \quad (4) \end{aligned}$$

with λ the triangular function. In this case, the pseudoscalar operator does not contribute.

As in the Hamiltonian (1), in Eqs. (2) and (4), the CKM matrix element V_{ub} appears in the combination $V_{ub}(1 + \epsilon_V^\ell)$. The lepton-flavor dependence of the effective couplings would manifest in different determinations of V_{ub} from channels involving different lepton species.

We discuss below how the experimental measurements constrain the parameter spaces.

Continuing with the semileptonic mode to the pion, in the large energy limit of the emitted pion, using Eq. (A13) for the weak matrix element, the decay distribution is expressed in terms of a single form factor ξ_π [50,51],

$$\begin{aligned} \frac{d\Gamma}{dE}(\bar{B} \rightarrow \pi \ell^- \bar{\nu}_\ell) &= \frac{G_F^2 |V_{ub}|^2 \lambda^{1/2}(m_B^2, m_\pi^2, q^2)}{64 m_B^2 \pi^3 q^2} \left(1 - \frac{m_\ell^2}{q^2}\right)^2 \xi_\pi^2(E) \\ &\times \left\{ \left| m_\ell (1 + \epsilon_V^\ell) + \frac{q^2 \epsilon_S^\ell}{m_b - m_u} \right|^2 (m_B^2 - m_\pi^2)^2 \left(\frac{m_B^2 + m_\pi^2 - q^2}{m_B^2}\right)^2 \right. \\ &\left. + \lambda(m_B^2, m_\pi^2, q^2) \left[\frac{1}{3} \left| m_\ell (1 + \epsilon_V^\ell) + \frac{4q^2}{m_B} \epsilon_T^\ell \right|^2 + \frac{2q^2}{3} \left| (1 + \epsilon_V^\ell) + \frac{4m_\ell}{m_B} \epsilon_T^\ell \right|^2 \right] \right\}, \quad (5) \end{aligned}$$

with $q^2 = m_B^2 + m_\pi^2 - 2m_B E$. While the full kinematical range for E is $m_\pi \leq E \leq \frac{m_B}{2} \left(1 + \frac{m_\pi^2}{m_B^2} - \frac{m_\ell^2}{m_B^2}\right)$, Eq. (5) only holds for large $E \simeq \frac{m_B}{2}$. This expression is useful if the distribution is independently measured for the three charged leptons, since the ratios

$$\frac{dR(\pi)^{\ell\ell'}}{dE} = \frac{d\Gamma(\bar{B} \rightarrow \pi \ell^- \bar{\nu}_\ell)}{dE} / \frac{d\Gamma(\bar{B} \rightarrow \pi \ell'^- \bar{\nu}_{\ell'})}{dE} \quad (6)$$

are free of hadronic uncertainties in this limit, and only involve combinations of the lepton-flavor dependent couplings $\epsilon_{V,S,T}^{\ell,\ell'}$.

III. FULLY DIFFERENTIAL ANGULAR DISTRIBUTIONS FOR $\bar{B} \rightarrow \rho(\rightarrow \pi\pi)\ell^- \bar{\nu}_\ell$ AND $\bar{B} \rightarrow a_1(\rightarrow \rho\pi)\ell^- \bar{\nu}_\ell$

The main sensitivity to the new operators in (1), in the modes $\bar{B} \rightarrow \rho(\rightarrow \pi\pi)\ell^- \bar{\nu}_\ell$ and $\bar{B} \rightarrow a_1(\rightarrow \rho\pi)\ell^- \bar{\nu}_\ell$, is in the four-dimensional differential decay distribution in the variables q^2 and in the angles θ , θ_V , and ϕ described in Fig. 1. For the ρ mode, the distribution is written as³

³Other angular structures appear in the differential distributions if a quark right-handed vector current is included in Eq. (1).

$$\begin{aligned}
\frac{d^4\Gamma(\bar{B} \rightarrow \rho(\rightarrow \pi\pi)\ell^-\bar{\nu}_\ell)}{dq^2 d\cos\theta d\phi d\cos\theta_V} &= \mathcal{N}_\rho |\vec{p}_\rho| \left(1 - \frac{m_\ell^2}{q^2}\right)^2 \{I_{1s}^\rho \sin^2\theta_V + I_{1c}^\rho \cos^2\theta_V + (I_{2s}^\rho \sin^2\theta_V + I_{2c}^\rho \cos^2\theta_V) \cos 2\theta \\
&+ I_3^\rho \sin^2\theta_V \sin^2\theta \cos 2\phi + I_4^\rho \sin 2\theta_V \sin 2\theta \cos \phi + I_5^\rho \sin 2\theta_V \sin \theta \cos \phi \\
&+ (I_{6s}^\rho \sin^2\theta_V + I_{6c}^\rho \cos^2\theta_V) \cos \theta + I_7^\rho \sin 2\theta_V \sin \theta \sin \phi\}, \tag{7}
\end{aligned}$$

with $\mathcal{N}_\rho = \frac{3G_F^2 |V_{ub}|^2 \mathcal{B}(\rho \rightarrow \pi\pi)}{128(2\pi)^4 m_B^2}$. This expression, together with the relation of the coefficient functions to the hadronic matrix elements, has been computed in the narrow width approximation, resulting in a factorization of the production and decay amplitude of the intermediate vector meson. The factorization is connected to the procedure adopted in the experimental analyses to select the contributions of the intermediate resonances [52].⁴ A $\pi\pi$ contribution considered as an improvement of the narrow width approximation

(NWA) has been investigated through the computation of the $B \rightarrow \pi\pi$ matrix elements in the kinematical regime of small dipion invariant mass and large energy, concluding that it represents a small effect [56–58].

For the $a_1(\rho\pi)$ channel, it is useful to provide the expressions for the modes where the final ρ is transversely (ρ_\perp) or longitudinally (ρ_\parallel) polarized, as specified in Appendix B. The expression of the four-dimensional distribution amplitude is

$$\begin{aligned}
\frac{d^4\Gamma(\bar{B} \rightarrow a_1(\rightarrow \rho_{\parallel(\perp)}\pi)\ell^-\bar{\nu}_\ell)}{dq^2 d\cos\theta d\phi d\cos\theta_V} &= \mathcal{N}_{a_1}^{|\parallel(\perp)} |\vec{p}_{a_1}| \left(1 - \frac{m_\ell^2}{q^2}\right)^2 \{I_{1s,|\parallel(\perp)}^{a_1} \sin^2\theta_V + I_{1c,|\parallel(\perp)}^{a_1} (3 + \cos 2\theta_V) \\
&+ (I_{2s,|\parallel(\perp)}^{a_1} \sin^2\theta_V + I_{2c,|\parallel(\perp)}^{a_1} (3 + \cos 2\theta_V)) \cos 2\theta \\
&+ I_{3,|\parallel(\perp)}^{a_1} \sin^2\theta_V \sin^2\theta \cos 2\phi + I_{4,|\parallel(\perp)}^{a_1} \sin 2\theta_V \sin 2\theta \cos \phi \\
&+ I_{5,|\parallel(\perp)}^{a_1} \sin 2\theta_V \sin \theta \cos \phi \\
&+ (I_{6s,|\parallel(\perp)}^{a_1} \sin^2\theta_V + I_{6c,|\parallel(\perp)}^{a_1} (3 + \cos 2\theta_V)) \cos \theta \\
&+ I_{7,|\parallel(\perp)}^{a_1} \sin 2\theta_V \sin \theta \sin \phi\}, \tag{8}
\end{aligned}$$

with the subscripts \perp, \parallel referring to the two ρ polarizations.

The coefficients $\mathcal{N}_{a_1}^{|\parallel(\perp)}$ read $\mathcal{N}_{a_1}^{|\parallel(\perp)} = \frac{3G_F^2 |V_{ub}|^2 \mathcal{B}(a_1 \rightarrow \rho_{\parallel(\perp)}\pi)}{128(2\pi)^4 m_B^2}$.

The separation of the ρ polarizations is an experimental challenge, which is justified in view of the different sensitivity of the angular coefficient functions to the NP operators. The unpolarized case is recovered by combining the expressions for the transverse and longitudinal ρ polarization. The NWA has been adopted also for the computation of the distribution (8) with the derivation of the relations of the angular coefficient functions in terms of $B \rightarrow a_1$ matrix elements. This is a more debatable procedure than for the ρ channel. Its motivation relies on the assumption that the experimental analyses can constrain the $\rho\pi$ invariant mass in a narrow range around the a_1 peak, separating the production and decay process of the intermediate resonance. Going beyond such a limit would require considering the $\rho\pi$ invariant mass distribution, with the $B \rightarrow a_1$ form factors extrapolated to different values of such a mass, with uncontrolled uncertainties. On the other hand, considering the three pion final state would include

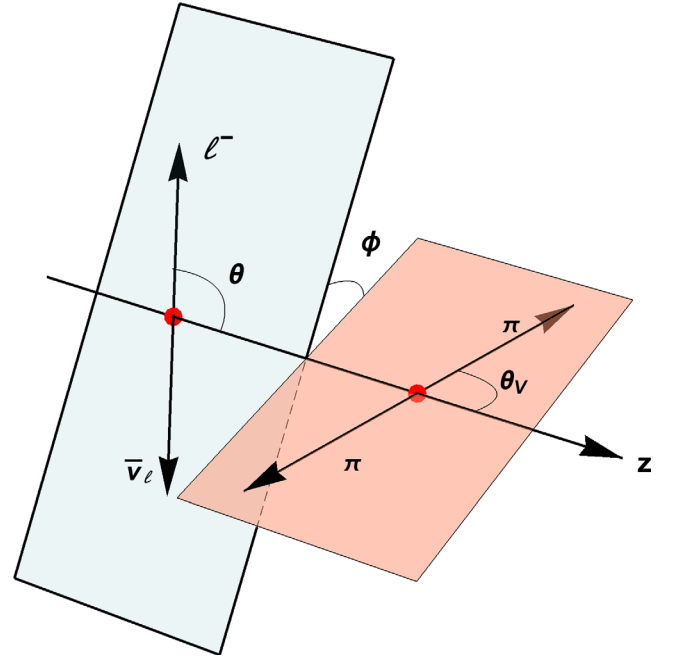


FIG. 1. Kinematics of the decay mode $\bar{B} \rightarrow \rho(\pi\pi)\ell^-\bar{\nu}_\ell$.

⁴Studies of the B_{c4} mode are in Refs. [53–55].

contributions from several resonances of various spin parity, affected in different ways from the NP operators when produced in semileptonic B modes.

The angular coefficient functions I_i^ρ and $I_i^{a_1}$ in Eqs. (7) and (8) can be written as

$$\begin{aligned}
 I_i &= |1 + \epsilon_V|^2 I_i^{\text{SM}} + |\epsilon_X|^2 I_i^{\text{NP},X} + |\epsilon_T|^2 I_i^{\text{NP},T} \\
 &\quad + 2\text{Re}[\epsilon_X(1 + \epsilon_V^*)] I_i^{\text{INT},X} + 2\text{Re}[\epsilon_T(1 + \epsilon_V^*)] I_i^{\text{INT},T} \\
 &\quad + 2\text{Re}[\epsilon_X \epsilon_T^*] I_i^{\text{INT},XT}, \quad (i = 1, \dots, 6), \\
 I_7 &= 2\text{Im}[\epsilon_X(1 + \epsilon_V^*)] I_7^{\text{INT},X} + 2\text{Im}[\epsilon_T(1 + \epsilon_V^*)] I_7^{\text{INT},T} \\
 &\quad + 2\text{Im}[\epsilon_X \epsilon_T^*] I_7^{\text{INT},XT}, \quad (9)
 \end{aligned}$$

with $X = P$ in case of ρ and $X = S$ in case of a_1 . The coefficient functions I_i^{SM} , I_i^{NP} , and I_i^{INT} , expressed in terms of helicity amplitudes, are collected in Tables II–IX of Appendix B, together with the relations of the helicity amplitudes to the hadron form factors.

Examining the angular coefficient functions and their expressions, several remarks are in order:

- (1) With the exception of I_7 , all angular coefficient functions do not vanish in SM and are sensitive to ϵ_V . Apart from such a dependence, we can identify structures useful to disentangle the effects of the other S, P, and T operators. In $B \rightarrow \rho \ell \bar{\nu}_\ell$, the functions $I_{1s}^\rho, I_{2s}^\rho, I_{2c}^\rho, I_{3s}^\rho, I_{4s}^\rho, I_{6s}^\rho$ do not depend on ϵ_P , as it can be inferred from Table III, and are sensitive only to the tensor operator. We denote these structures as belonging to set A, while set B comprises the remaining ones. An analogous situation occurs for the corresponding quantities in $B \rightarrow a_1(\rho_{\parallel}) \ell \bar{\nu}_\ell$, which do not depend on ϵ_S (Table VI), while in $B \rightarrow a_1(\rho_{\perp}) \ell \bar{\nu}_\ell$, the functions $I_{1c,\perp}^{a_1}, I_{2s,\perp}^{a_1}, I_{2c,\perp}^{a_1}, I_{3,\perp}^{a_1}, I_{4,\perp}^{a_1}, I_{6c,\perp}^{a_1}$ are insensitive to the scalar operator (Table VII).
- (2) In the absence of the tensor operator, the ρ and a_1 modes give complementary information on the pseudoscalar P (in the ρ channel) and scalar S (in a_1) operators, together with the purely leptonic mode (sensitive to P) and $B \rightarrow \pi$ mode (sensitive to S).
- (3) There are angular coefficient functions that depend only on the helicity amplitudes H_{\pm} , not on H_0 and H_i . These affect observables corresponding to the transversely polarized W , hence to transverse ρ in $B \rightarrow \rho \ell \bar{\nu}_\ell$ and transverse a_1 in $B \rightarrow a_1 \ell \bar{\nu}_\ell$. Such observables depend on ϵ_T , not on ϵ_P (in the ρ mode) or ϵ_S (in the a_1 mode).
- (4) In the large energy limit of the light meson, the form factors parametrizing the $B \rightarrow \rho(a_1)$ weak matrix elements can be written in terms of two form factors, $\xi_{\perp}^\rho(\xi_{\perp}^{a_1})$ and $\xi_{\parallel}^\rho(\xi_{\parallel}^{a_1})$, defined by the relations (A14) and (A15). In this limit, several angular coefficients depend only on the form factor ξ_{\perp} ; others involve

both ξ_{\perp} and ξ_{\parallel} . The coefficients depending only on $\xi_{\perp}^{\rho,a_1}(E)$ are:

- (a) in the $B \rightarrow \rho(770)$ mode: $I_{1s}^\rho, I_{2s}^\rho, I_{3s}^\rho$ and I_{6s}^ρ ;
- (b) in the $B \rightarrow a_1(1260)$ mode:
 - (i) for final ρ longitudinally polarized, $I_{1s,\parallel}^{a_1}, I_{2s,\parallel}^{a_1}, I_{3,\parallel}^{a_1}$, and $I_{6s,\parallel}^{a_1}$,
 - (ii) for ρ transversely polarized, $I_{1c,\perp}^{a_1}, I_{2c,\perp}^{a_1}, I_{3,\perp}^{a_1}$, and $I_{6c,\perp}^{a_1}$.

When a single form factor is involved, ratios of coefficient functions are free of hadronic uncertainties (in the large energy limit).

The conclusion is that, measuring the differential angular distribution and reconstructing the angular coefficient functions, it is possible to define sets of observables particularly sensitive to different NP terms in (1). This would allow us to determine the new couplings ϵ_i^ℓ and carry out tests, e.g., of LFU, comparing results obtained in the μ and τ modes.

IV. CONSTRAINTS ON THE EFFECTIVE COUPLINGS AND $\bar{B} \rightarrow \rho \ell^- \bar{\nu}_\ell$ OBSERVABLES

We want to present examples of the possible effects of the NP operators in (1) in $\bar{B} \rightarrow \rho \ell^- \bar{\nu}_\ell$, identifying the most sensitive observables. For that, we constrain the space of the new couplings using the available data and a set of hadronic quantities. More precise experimental measurements or more accurate theoretical determinations of the hadronic quantities, when available in the future, will modify the ranges of the couplings, but the strategy and the overall picture we are presenting will remain valid.

The couplings $\epsilon_V^\mu, \epsilon_P^\mu, \epsilon_T^\mu$ are constrained by the measurements $\mathcal{B}(\bar{B}^0 \rightarrow \pi^+ \ell^- \bar{\nu}_\ell) = (1.50 \pm 0.06) \times 10^{-4}$ and $\mathcal{B}(\bar{B}^0 \rightarrow \rho^+ \ell^- \bar{\nu}_\ell) = (2.94 \pm 0.21) 10^{-4}$ [59], together with $\mathcal{B}(B^- \rightarrow \mu^- \bar{\nu}_\mu) = (6.46 \pm 2.2 \pm 1.60) \times 10^{-7}$ (and 90% probability interval $[2.0, 10.7] \times 10^{-7}$) [60]. For e and τ , the results for the purely leptonic modes are $\mathcal{B}(B^- \rightarrow e^- \bar{\nu}_e) < 9.8 \times 10^{-7}$ and $\mathcal{B}(B^- \rightarrow \tau^- \bar{\nu}_\tau) = (1.09 \pm 0.24) \times 10^{-4}$ [59]. The upper bound $\mathcal{B}(\bar{B}^0 \rightarrow \pi^+ \tau^- \bar{\nu}_\tau) < 2.5 \times 10^{-4}$ has also been established [61]. We use the $B \rightarrow \pi$ form factors given in Appendix C, obtained by interpolating the light-cone sum rule results at low q^2 computed in Refs. [62,63] with the lattice QCD results at large values of q^2 averaged by HFLAG [64]. For the $B \rightarrow \rho$ transition, we use the form factors in Ref. [65], which update previous light-cone sum rule computations [66] and extrapolate the low q^2 determination to the full kinematical range.

In the case of μ , the parameter space for the NP couplings, displayed in Fig. 2, is found by imposing that the purely leptonic branching ratio (BR) is in the range $[2.0, 10.7] \times 10^{-7}$ and that the semileptonic $\bar{B} \rightarrow \pi$ and $\bar{B} \rightarrow \rho$ branching fractions are compatible within 2σ with measurement. The benchmark point shown in Fig. 2 is chosen in the region of the smallest

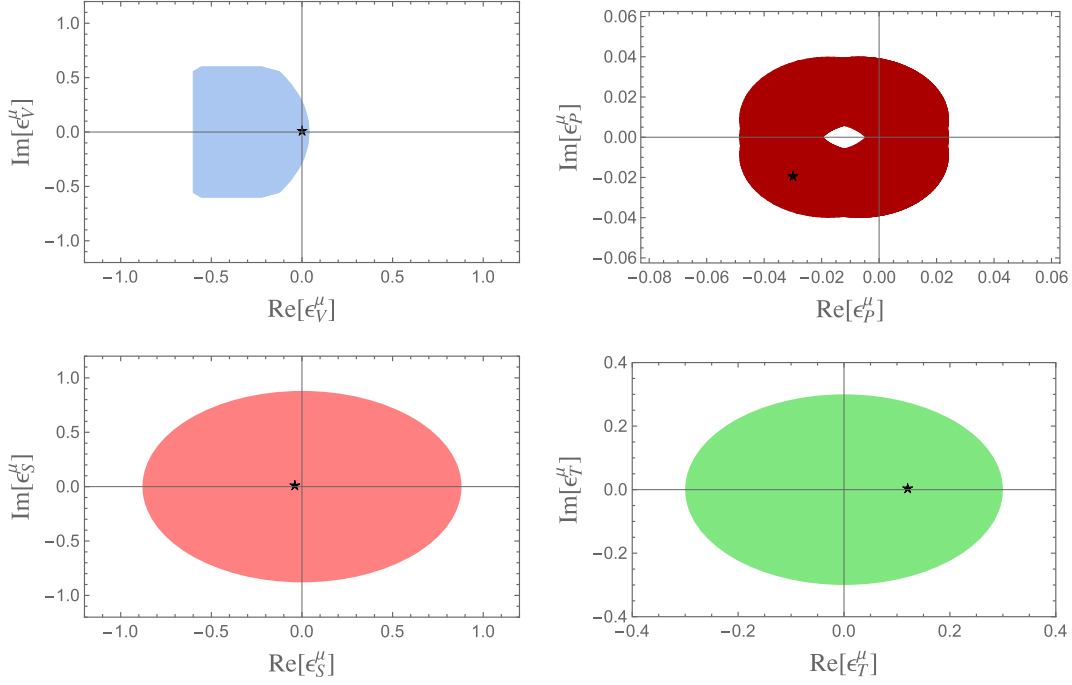


FIG. 2. Allowed regions for the couplings ϵ_V^μ , ϵ_P^μ , ϵ_S^μ , and ϵ_T^μ . The colors distinguish the various couplings. The stars correspond to the benchmark points, chosen in the region of minimum χ^2 : $(\text{Re}[\epsilon_V^\mu], \text{Im}[\epsilon_V^\mu]) = (0, 0)$, $(\text{Re}[\epsilon_P^\mu], \text{Im}[\epsilon_P^\mu]) = (-0.03, -0.02)$, $(\text{Re}[\epsilon_T^\mu], \text{Im}[\epsilon_T^\mu]) = (0.12, 0)$, and $(\text{Re}[\epsilon_S^\mu], \text{Im}[\epsilon_S^\mu]) = (-0.04, 0)$, with $|V_{ub}| = 3.5 \times 10^{-3}$.

$$\chi^2 = \sum_i^3 \left(\frac{\mathcal{B}_i^{\text{th}} - \mathcal{B}_i^{\text{exp}}}{\Delta \mathcal{B}_i^{\text{exp}}} \right)^2 \quad (10)$$

for the three modes, varying $|V_{ub}|$ in $[3.5, 4.4] \times 10^{-3}$. Specifically, in the region of smallest χ^2 , we have selected the points in the parameter space having $\epsilon_V^\ell = 0$ and all the other $\epsilon_A^\ell \neq 0$, with $A = S, P, T$. Our benchmark point is the

one minimizing χ^2 . We set $\epsilon_V^\ell = 0$ to maximize the sensitivity to the other NP couplings.

For the τ modes, due to the smaller number of experimental constraints, we consider a limited parameter space setting $\epsilon_V^\tau = 0$ and $\epsilon_S^\tau = 0$ from the beginning. The region for ϵ_P^τ in Fig. 3 (left panel) is constrained by imposing the compatibility of $\mathcal{B}(B^- \rightarrow \tau^- \bar{\nu}_\tau)$ with measurement. We have checked that $\frac{\mathcal{B}(B^- \rightarrow \mu^- \bar{\nu}_\mu)}{\mathcal{B}(B^- \rightarrow \tau^- \bar{\nu}_\tau)}$ lies within the experimental

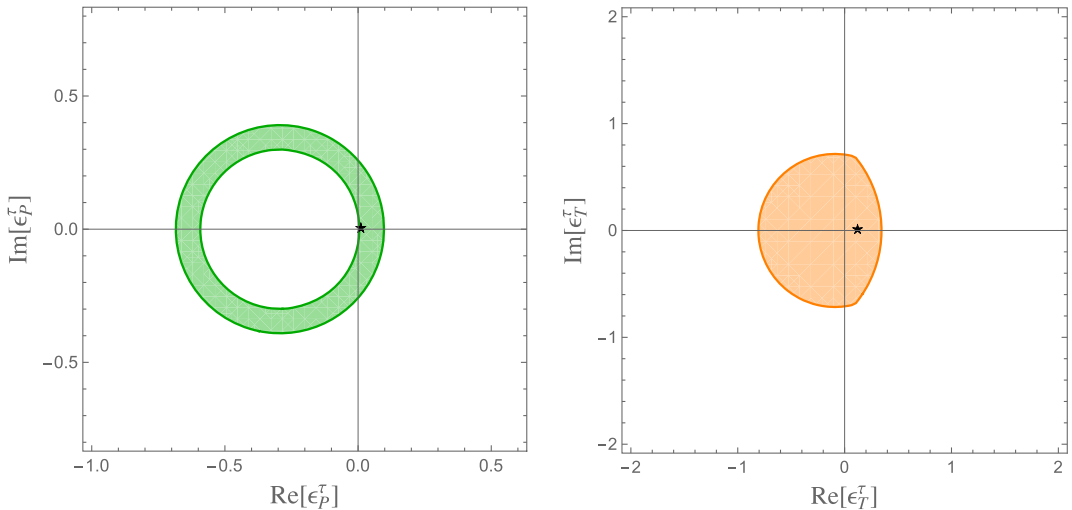


FIG. 3. Allowed regions for the couplings ϵ_P^τ and ϵ_T^τ . The stars correspond to the benchmark points chosen setting $\epsilon_V^\tau = 0$ and $\epsilon_S^\tau = 0$: $(\text{Re}[\epsilon_P^\tau], \text{Im}[\epsilon_P^\tau]) = (0.01, 0)$ and $(\text{Re}[\epsilon_T^\tau], \text{Im}[\epsilon_T^\tau]) = (0.12, 0)$.

range when ϵ_V^μ and ϵ_P^μ are varied in their ranges. The region for ϵ_T^τ (right panel) is obtained by imposing the experimental upper bound for $\mathcal{B}(\bar{B}^0 \rightarrow \pi^+ \tau^- \bar{\nu}_\tau)$ together with the limit for $R_\pi = \frac{\mathcal{B}(\bar{B}^0 \rightarrow \pi^+ \tau^- \bar{\nu}_\tau)}{\mathcal{B}(\bar{B}^0 \rightarrow \pi^+ \mu^- \bar{\nu}_\mu)}$. In the wide resulting region, we set the range for ϵ_T^τ , with the parameters for the muon fixed at their benchmark values; then, we fix a benchmark point to provide an example of NP effects.

We can now compare observables in the SM and NP. The angular coefficient functions I_{1s}^ρ , I_{2s}^ρ , I_{2c}^ρ , I_3^ρ , I_4^ρ , and I_{6s}^ρ , independent of ϵ_P , are shown in Fig. 4, setting ϵ_T^μ at a benchmark point. The zero in $I_{2s}^\rho(q^2)$ is absent in the SM and appears in NP. The other coefficient functions are drawn in Fig. 5, and also in this case, there is a zero in $I_{6c}^\rho(q^2)$ which is absent in the SM. The function I_7^ρ vanishes in the SM and is only sensitive to the imaginary part of the NP couplings; it is shown in Fig. 6. The angular functions

for the τ modes are in Figs. 7 and 8; I_7^τ vanishes since at the chosen benchmark point all the NP couplings ϵ^τ are real. Also in this mode, the coefficient I_{6c}^ρ has a zero not appearing in the SM.

The measurement of the angular coefficients functions allows us to determine the new couplings. Let us consider the ratios

$$R_{2s/1s}^\rho(q^2) = \frac{I_{2s}^\rho(q^2)}{I_{1s}^\rho(q^2)}, \quad (11)$$

$$R_{2s/1s}^{a_1,||}(q^2) = \frac{I_{2s,||}^{a_1}(q^2)}{I_{1s,||}^{a_1}(q^2)}, \quad (12)$$

and $R_{2s/1s}^{a_1,||} = R_{2c/1c}^{a_1,\perp}$. In the SM, $R_{2s/1s}^\rho$ is form factor independent. In NP, it is still form factor independent in

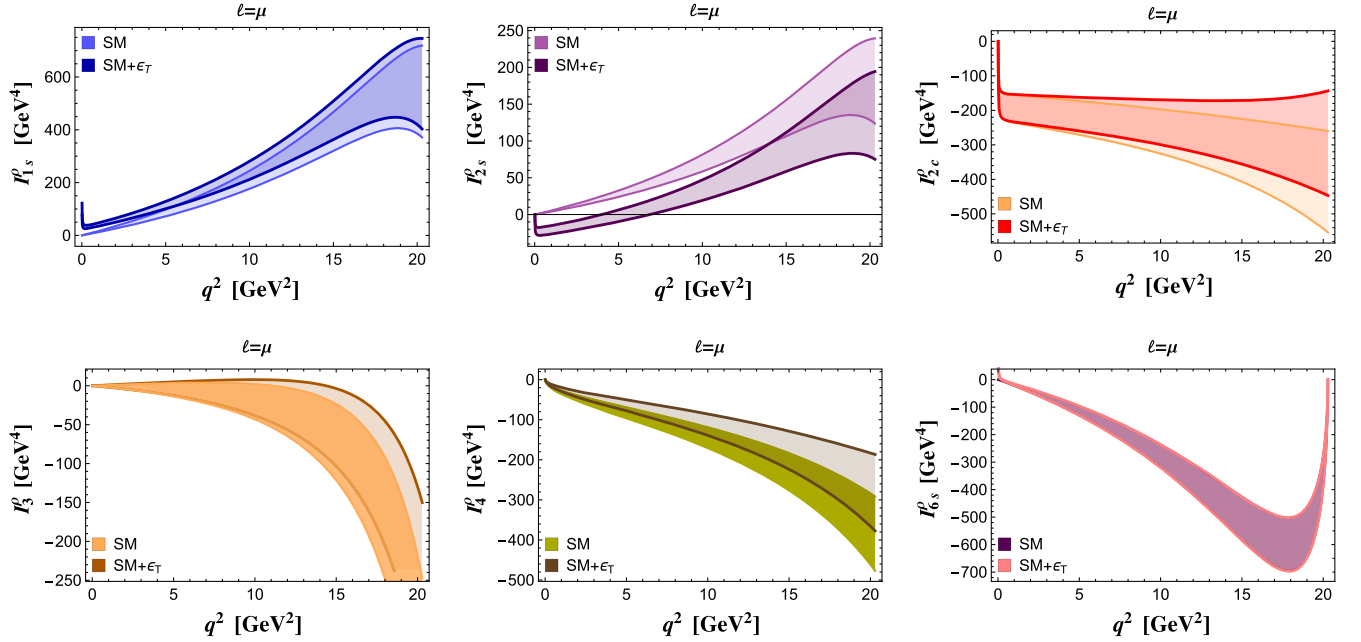


FIG. 4. $\bar{B} \rightarrow \rho(\pi\pi)\mu^-\bar{\nu}_\mu$ mode: angular coefficient functions $I_i^\rho(q^2)$ in set A, for the SM and NP at the benchmark point. A zero in $I_{2s}^\rho(q^2)$ appears in NP.

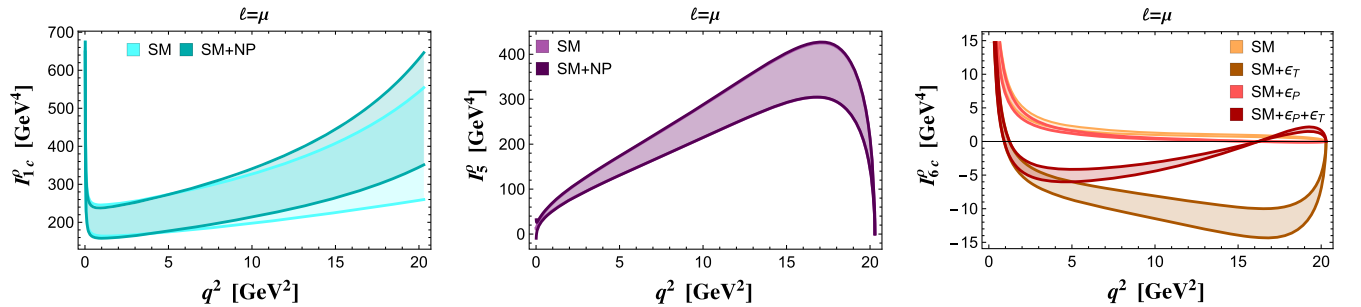


FIG. 5. $\bar{B} \rightarrow \rho(\pi\pi)\mu^-\bar{\nu}_\mu$ mode: angular coefficient functions (set B) $I_{1c}^\rho(q^2)$ (left), $I_5^\rho(q^2)$ (middle), and $I_{6c}^\rho(q^2)$ (right) for the SM and NP at the benchmark point.

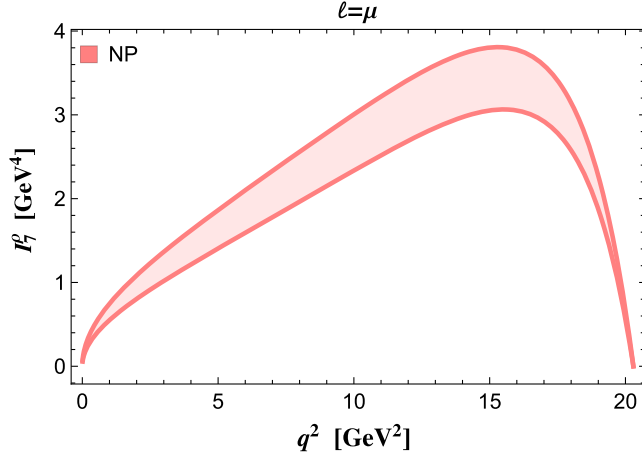


FIG. 6. $\bar{B} \rightarrow \rho(\pi\pi)\mu^-\bar{\nu}_\mu$ mode: angular coefficient function $I_7^\rho(q^2)$ in NP with the pseudoscalar operator at the benchmark point.

the large energy limit, where I_{2s}^ρ and I_{1s}^ρ depend on ξ_\perp^ρ . As shown in Fig. 9, the ratio (11) has a zero in the NP, not in the SM, of which the position $q_{0,\rho}^2$ has a weak form factor effect and depends only on $|\epsilon_T^\mu|$. In the large energy limit, we have

$$|\epsilon_T^\mu|^2 = \frac{q_{0,\rho}^2 \lambda(m_B^2, m_\rho^2, q_{0,\rho}^2) + 2m_B^2 m_\rho^2}{16m_B^2 \lambda(m_B^2, m_\rho^2, q_{0,\rho}^2) + 2q_{0,\rho}^2 m_\rho^2}. \quad (13)$$

Analogously, for the $(a_1)_\parallel$ mode [and for $(a_1)_\perp$ considering $R_{2c/1c}$], we have

$$|\epsilon_T^\mu|^2 = \frac{q_{0,a_1}^2 \lambda(m_B^2, m_{a_1}^2, q_{0,a_1}^2) + 2m_B^2 m_{a_1}^2}{16m_B^2 \lambda(m_B^2, m_{a_1}^2, q_{0,a_1}^2) + 2q_{0,a_1}^2 m_{a_1}^2}. \quad (14)$$

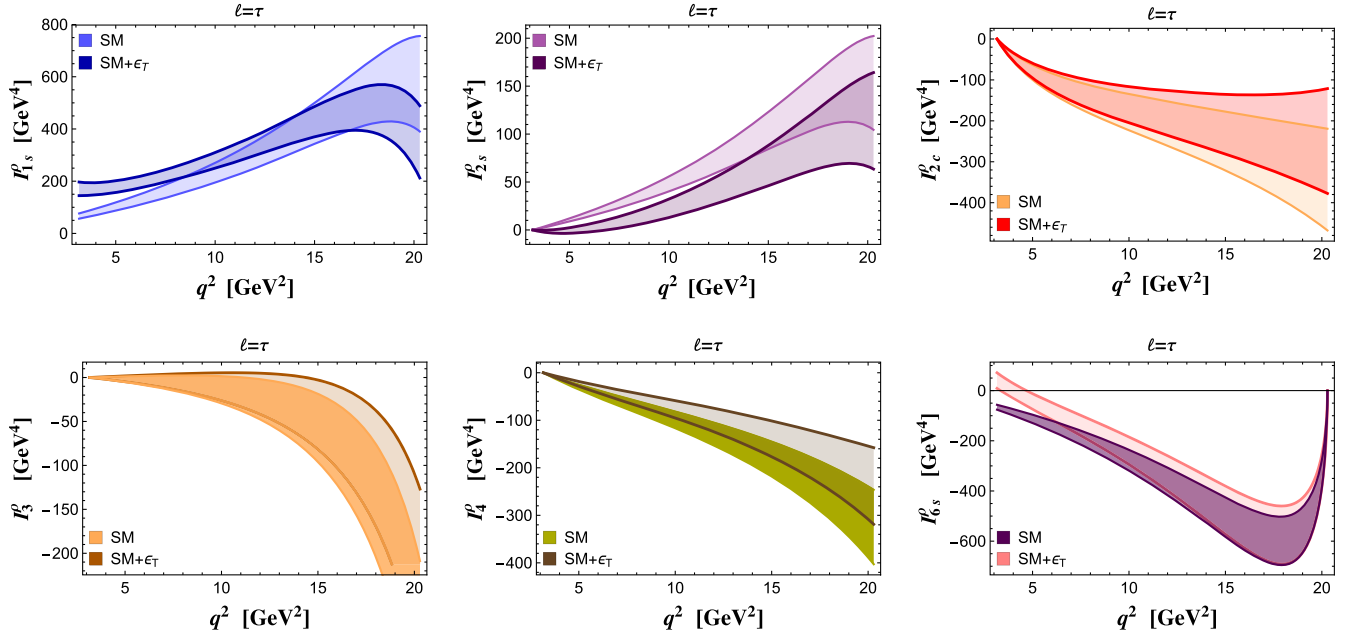


FIG. 7. $\bar{B} \rightarrow \rho(\pi\pi)\tau^-\bar{\nu}_\tau$ mode: angular coefficient functions $I_i^\rho(q^2)$ in set A for the SM and NP at the benchmark point.

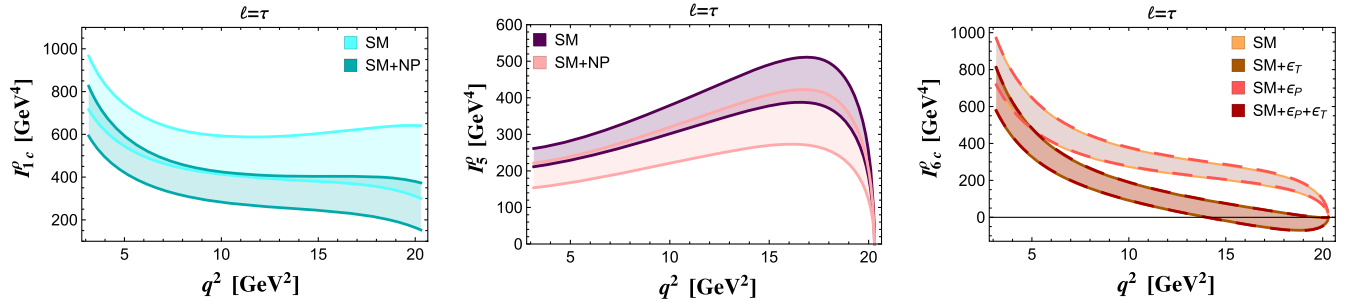


FIG. 8. $\bar{B} \rightarrow \rho(\pi\pi)\tau^-\bar{\nu}_\tau$ mode: angular coefficient functions (set B) $I_{1c}^\rho(q^2)$ (left), $I_5^s(q^2)$ (middle), and $I_{6c}^\rho(q^2)$ (right) for the SM and NP at the benchmark point.

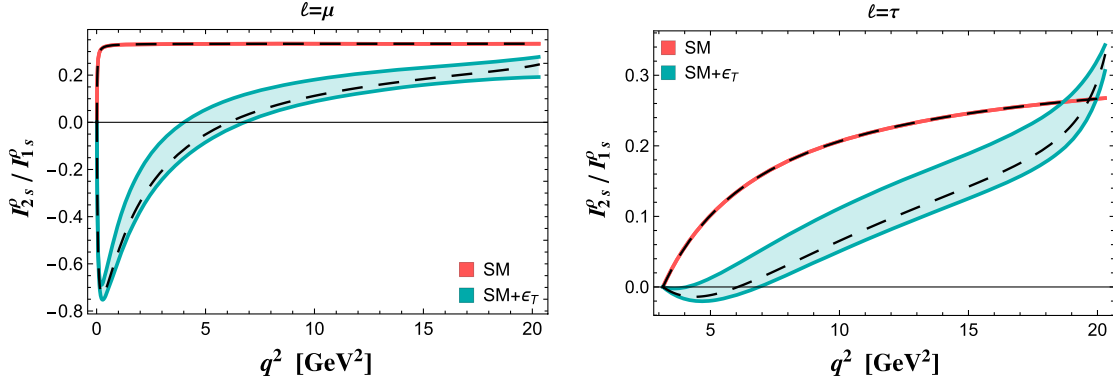


FIG. 9. Ratio $R_{2s/1s}^\rho$ in (11) the modes $\bar{B} \rightarrow \rho(\pi\pi)\mu^-\bar{\nu}_\mu$ (left) and $\bar{B} \rightarrow \rho(\pi\pi)\tau^-\bar{\nu}_\mu$ (right), in the SM and NP with the tensor operator at the benchmark point. The dashed lines correspond to the large energy limit result (extrapolated to the full q^2 range).

The positions of the zeros in two modes are related, see Fig. 10, and their independent measurement would provide a connection with the tensor operator.

Another suitable quantity is the angular coefficient function I_{6c}^ρ shown in the right panel of Fig. 5 in the SM and NP, which is sensitive to ϵ_V , ϵ_P , ϵ_T . At our benchmark point, $\epsilon_V \simeq 0$; hence, we keep only the ϵ_P and ϵ_T dependence:

$$(I_{6c}^\rho)|_{\epsilon_V \simeq 0} = (-2H_t^\rho) \left[4H_0^\rho m_\ell^2 - \text{Re}[\epsilon_T] H_L^{\text{NP},\rho} m_\ell \sqrt{q^2} \right. \\ \left. + 4\text{Re}[\epsilon_P] H_0^\rho \frac{m_\ell}{m_b + m_u} q^2 \right. \\ \left. - H_L^{\text{NP},\rho} \text{Re}[\epsilon_P \epsilon_T^*] \frac{(q^2)^{3/2}}{m_b + m_u} \right]. \quad (15)$$

Considering the q^2 dependence of the helicity amplitudes in Appendix B, we have the following possibilities:

- (i) No NP, i.e., $\epsilon_P = \epsilon_T = 0$. In this case, $I_{6c}^\rho = -8H_t^\rho H_0^\rho m_\ell^2$ does not have a zero, as shown in Fig. 5 (right panel).

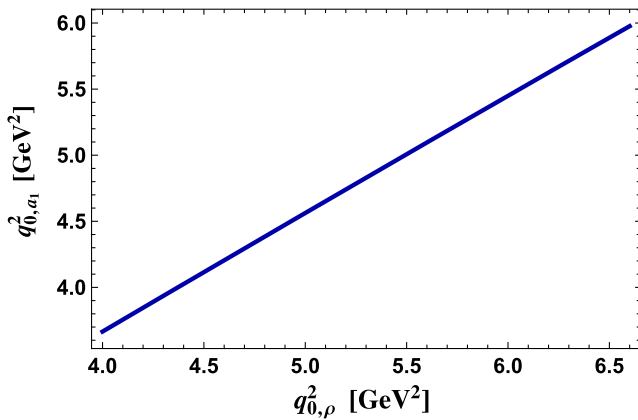


FIG. 10. Relation between the position of the zeroes q_0^2 of the ratios (11) and (12) for the $B \rightarrow \rho$ and $B \rightarrow a_1$ modes, respectively.

- (ii) NP with $\epsilon_T = 0$ and $\epsilon_P \neq 0$. This gives $(I_{6c}^\rho)|_{\epsilon_T \simeq 0} = (-8H_t^\rho H_0^\rho m_\ell) [m_\ell + \text{Re}[\epsilon_P] \frac{q^2}{m_b + m_u}]$, with a zero at

$$q_0^2 = -\frac{m_b + m_u}{m_\ell} \frac{1}{\text{Re}[\epsilon_P]}. \quad (16)$$

This position is form factor independent; its measurement would result in a determination of $\text{Re}[\epsilon_P]$. In the left panel of Fig. 11, we show I_{6c}^ρ enlarging the region where the zero is present for the benchmark $\text{Re}[\epsilon_P]$, and in the middle panel, we display q_0^2 vs $\text{Re}[\epsilon_P]$ in the whole range for the coupling.

- (iii) NP with $\epsilon_P = 0$ and $\epsilon_T \neq 0$, and $(I_{6c}^\rho)|_{\epsilon_P \simeq 0} = (-2H_t^\rho) [4H_0^\rho m_\ell^2 - \text{Re}[\epsilon_T] H_L^{\text{NP},\rho} m_\ell \sqrt{q^2}]$. The zero is present if $\text{Re}[\epsilon_T] > 0$. The position has a form factor dependence, as shown in Fig. 11 (right panel).
- (iv) NP with both $\epsilon_P \neq 0$ and $\epsilon_T \neq 0$. In this case, both real and imaginary parts of ϵ_P and ϵ_T are involved. One can notice from Fig. 5 that it is possible to have two zeros, nearly coinciding with those found in the previous two cases.

Integrating the four-dimensional differential decay distribution, several observables can be constructed:

- (i) q^2 -dependent forward-backward (FB) lepton asymmetry,

$$A_{\text{FB}}(q^2) = \left[\int_0^1 d\cos\theta \frac{d^2\Gamma}{dq^2 d\cos\theta} \right. \\ \left. - \int_{-1}^0 d\cos\theta \frac{d^2\Gamma}{dq^2 d\cos\theta} \right] \bigg/ \frac{d\Gamma}{dq^2}, \quad (17)$$

which is given in terms of the angular coefficient functions as

$$A_{\text{FB}}(q^2) = \frac{3(I_{6c}^\rho + 2I_{6s}^\rho)}{6I_{1c}^\rho + 12I_{1s}^\rho - 2I_{2c}^\rho - 4I_{2s}^\rho}. \quad (18)$$

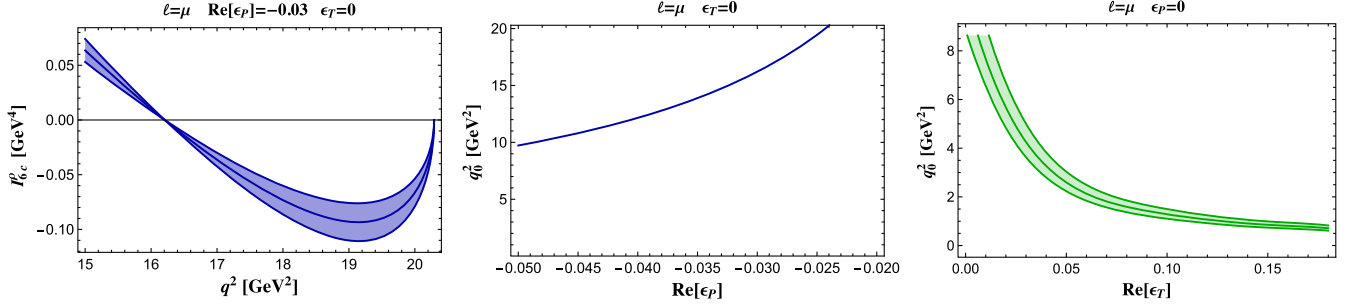


FIG. 11. $\bar{B} \rightarrow \rho(\pi\pi)\mu^-\bar{\nu}_\mu$ mode: coefficient function $I_{6c}^\rho(q^2)$ (left) and position q_0^2 varying $\text{Re}(\epsilon_P)$ with $\epsilon_T = 0$ (middle panel) and $\text{Re}(\epsilon_T)$ with $\epsilon_P = 0$ (right).

- (ii) Transverse forward-backward (TFB) asymmetry, the FB asymmetry for transversely polarized ρ , reading in terms of the angular coefficient functions as

$$A_{\text{FB}}^T(q^2) = \frac{3I_{6s}^\rho}{6I_{1s}^\rho - 2I_{2s}^\rho}. \quad (19)$$

For $\ell = \mu$, the asymmetries A_{FB} and A_{FB}^T are shown in Fig. 12, and for $\ell = \tau$, they are shown in Fig. 14. In the case of NP, the zero of A_{FB} in the τ mode is shifted. Moreover, A_{FB}^T is very sensitive to the new operators, and in the case of τ , it has a zero not present in the SM. This is related to I_{6s}^ρ , with a zero in NP and not in the SM.

- (iii) Observables sensitive to the ρ polarization. We consider the differential branching ratio for longitudinally (L) and transversely (T) polarized ρ as a function of q^2 or of one of the two angles θ , θ_V : $d\mathcal{B}_{L(T)}/dq^2$, $d\mathcal{B}_{L(T)}/d\cos\theta$ and $d\mathcal{B}_{L(T)}/d\cos\theta_V$. These observables are depicted for $\ell = \mu$ and for $\ell = \tau$ in Figs. 13 and 15, respectively.

Among all these quantities, the ones corresponding to transversely polarized ρ depend only on ϵ_T , as stressed in the legends of the corresponding figures.

Integrating the distributions, we obtain in the SM the longitudinal and transverse polarization fractions and the branching fractions:

$$F_L(\bar{B} \rightarrow \rho\mu^-\bar{\nu}_\mu)|_{\text{SM}} = 0.52 \pm 0.15$$

$$F_T(\bar{B} \rightarrow \rho\mu^-\bar{\nu}_\mu)|_{\text{SM}} = 0.48 \pm 0.11$$

$$\mathcal{B}(\bar{B}^0 \rightarrow \rho^+\mu^-\bar{\nu}_\mu)|_{\text{SM}} = (3.37 \pm 0.52) \times 10^{-4} \times \left(\frac{|V_{ub}|}{0.0035}\right)^2, \quad (20)$$

$$F_L(\bar{B} \rightarrow \rho\tau^-\bar{\nu}_\tau)|_{\text{SM}} = 0.50 \pm 0.13$$

$$F_T(\bar{B} \rightarrow \rho\tau^-\bar{\nu}_\tau)|_{\text{SM}} = 0.50 \pm 0.12$$

$$\mathcal{B}(\bar{B}^0 \rightarrow \rho^+\tau^-\bar{\nu}_\tau)|_{\text{SM}} = (1.80 \pm 0.25) \times 10^{-4} \times \left(\frac{|V_{ub}|}{0.0035}\right)^2. \quad (21)$$

For the $B \rightarrow \pi$ mode, we have

$$\mathcal{B}(\bar{B}^0 \rightarrow \pi^+\mu^-\bar{\nu}_\mu)|_{\text{SM}} = (1.5 \pm 0.1) \times 10^{-4} \times \left(\frac{|V_{ub}|}{0.0035}\right)^2$$

$$\mathcal{B}(\bar{B}^0 \rightarrow \pi^+\tau^-\bar{\nu}_\tau)|_{\text{SM}} = (0.92 \pm 0.06) \times 10^{-4} \times \left(\frac{|V_{ub}|}{0.0035}\right)^2. \quad (22)$$

The ratios

$$R_\pi = \frac{\mathcal{B}(\bar{B} \rightarrow \pi\tau^-\bar{\nu}_\tau)}{\mathcal{B}(\bar{B} \rightarrow \pi\ell^-\bar{\nu}_\ell)}, \quad R_\rho = \frac{\mathcal{B}(\bar{B} \rightarrow \rho\tau^-\bar{\nu}_\tau)}{\mathcal{B}(\bar{B} \rightarrow \rho\ell^-\bar{\nu}_\ell)} \quad (23)$$

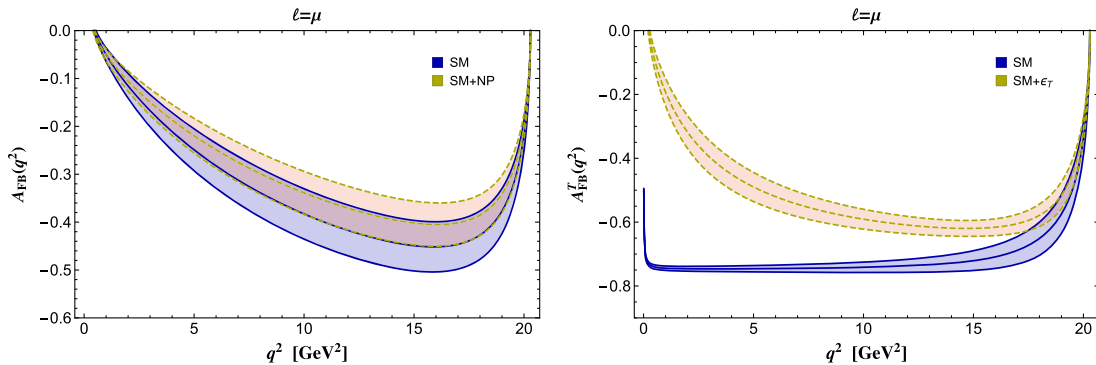


FIG. 12. $\bar{B} \rightarrow \rho\mu^-\bar{\nu}_\mu$ mode: forward-backward lepton asymmetry (17) and (19) in the SM and NP at the benchmark point.

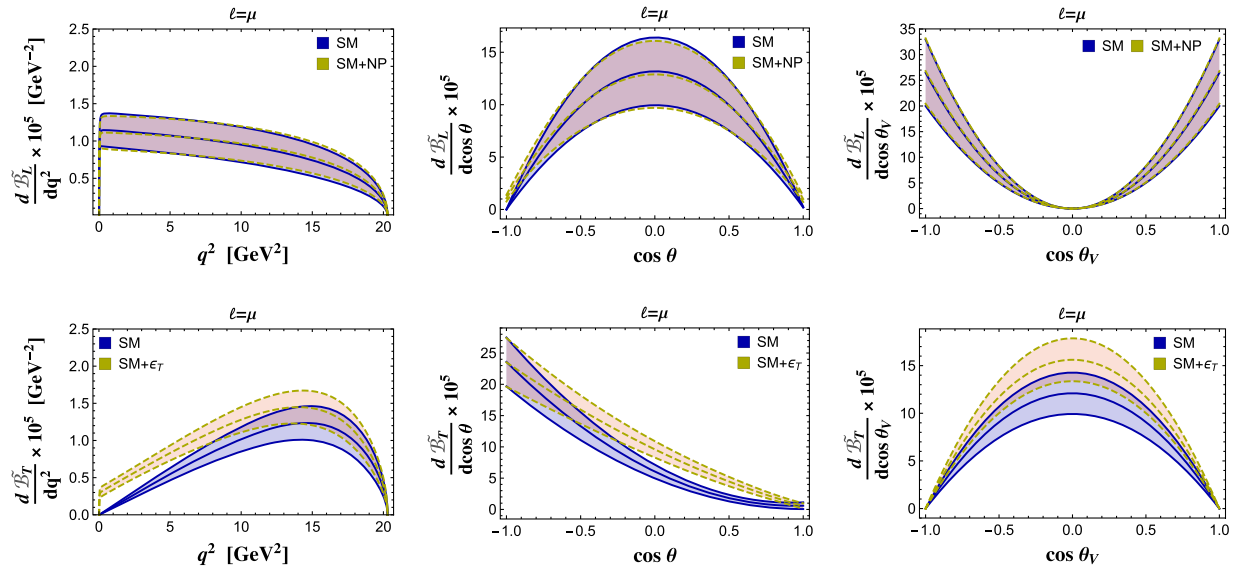


FIG. 13. $\bar{B} \rightarrow \rho \mu^- \bar{\nu}_\mu$ mode: distributions $d\tilde{B}_L/dq^2$, $d\tilde{B}_L/d \cos \theta$, and $d\tilde{B}_L/d \cos \theta_V$ (first line) and $d\tilde{B}_T/dq^2$, $d\tilde{B}_T/d \cos \theta$, and $d\tilde{B}_T/d \cos \theta_V$ (second line), with $\tilde{B} = B/B(\rho \rightarrow \pi\pi)$, in the SM and NP at the benchmark point.

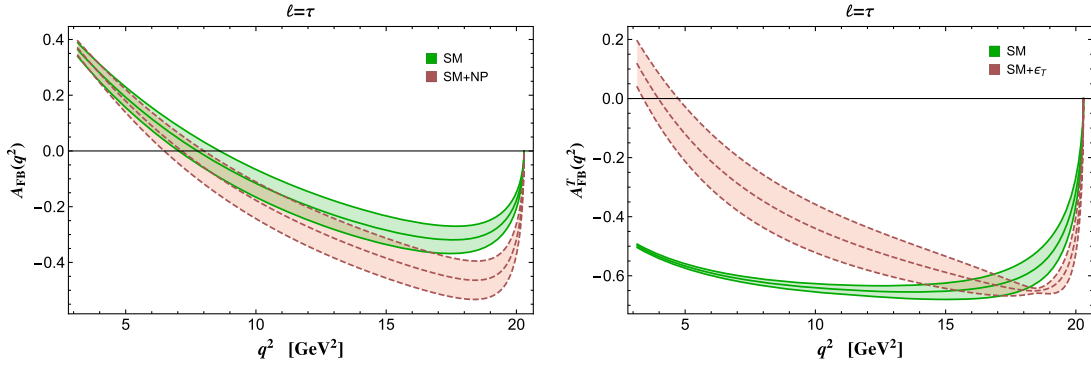


FIG. 14. $\bar{B} \rightarrow \rho \tau^- \bar{\nu}_\tau$ mode: asymmetries (17) and (19) in the SM and NP at the benchmark point.

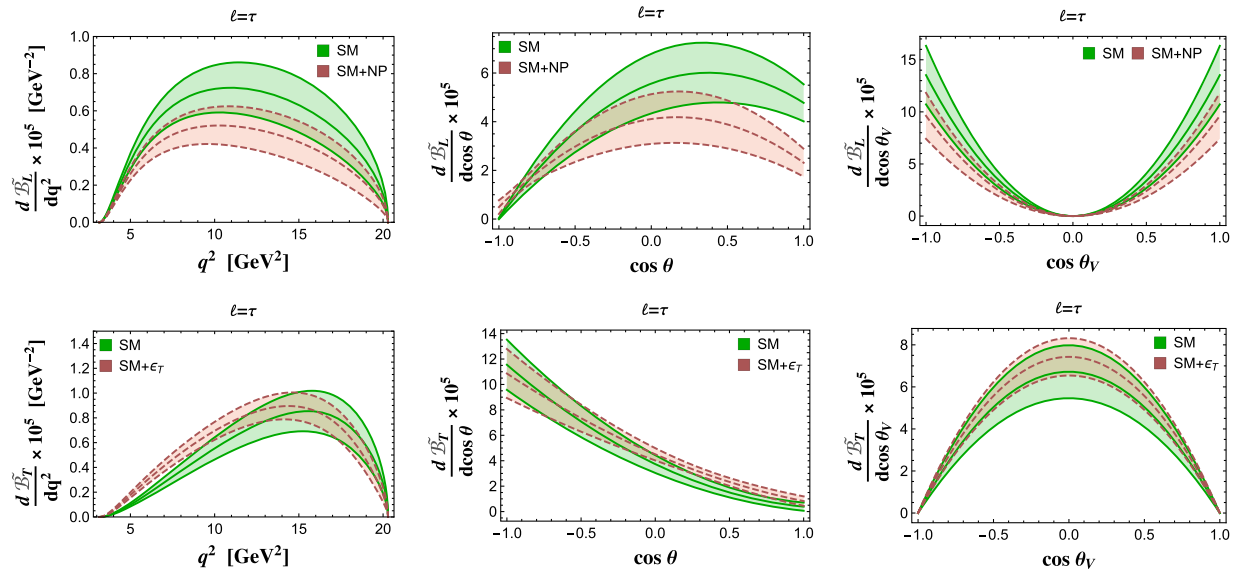


FIG. 15. $\bar{B} \rightarrow \rho \tau^- \bar{\nu}_\tau$ mode: distributions $d\tilde{B}_L/dq^2$, $d\tilde{B}_L/d \cos \theta$, and $d\tilde{B}_L/d \cos \theta_V$ (first line) and $d\tilde{B}_T/dq^2$, $d\tilde{B}_T/d \cos \theta$ and $d\tilde{B}_T/d \cos \theta_V$ (second line), with $\tilde{B} = B/B(\rho \rightarrow \pi\pi)$, in the SM and NP at the benchmark point.

TABLE I. Ratios R_π and R_ρ in Eq. (23) in the SM and in NP at the benchmark point.

	SM	NP (benchmark point)
R_π	0.60 ± 0.01	0.75 ± 0.02
R_ρ	0.53 ± 0.02	0.49 ± 0.02

are modified by the new physics operators in (1). The results in the SM and NP are collected in Table I, with the errors obtained by considering the uncertainties in the hadronic form factors. The deviations are correlated when the new operators are included in the effective Hamiltonian, and, as shown in Fig. 16, large effects are possible in corners of the parameter space of the new effective couplings.

Concerning R_π in the SM, the value $R_\pi = 0.641(17)$ is obtained using lattice form factors at large q^2 [67], the range $[0.654, 0.764]$ is found in Ref. [68], $R_\pi = 0.7$ together with $R_\rho \simeq 0.573$ is found using form factors computed in perturbative QCD [69], and $R_\pi \simeq 0.731$ and

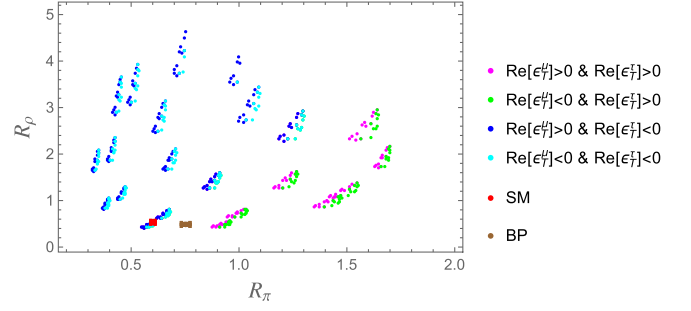


FIG. 16. Correlation between R_ρ and R_π in Eq. (23) with only the tensor operator added to the SM effective Hamiltonian. The colors correspond to the different signs of $\text{Re}(\epsilon_T^\mu)$ and $\text{Re}(\epsilon_T^\tau)$ in the full range of the parameter space. The red and brown points are the SM and NP results at the benchmark point, respectively.

$R_\rho \simeq 0.585$ are quoted in Ref. [70]. The effect of a new charged Higgs reduces the SM result for R_π and R_ρ [71]. Considering a single NP operator per time, values for R_π up to about four are obtained in Ref. [68], the range $[0.5, 1.38]$ is found in Ref. [69], while the inclusion only of the

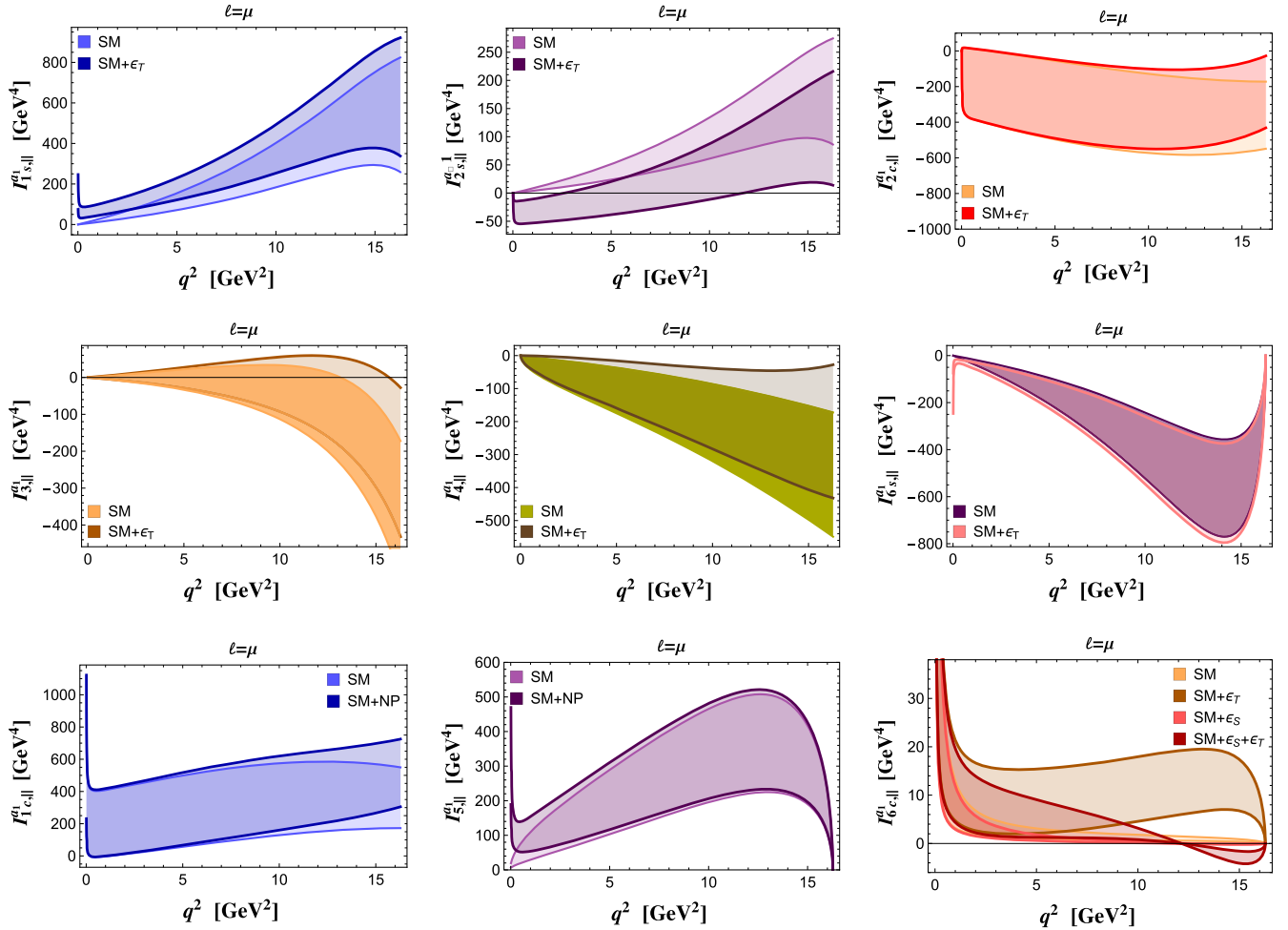


FIG. 17. $\bar{B} \rightarrow a_1(\rho|\pi)\mu^-\bar{\nu}_\mu$ mode: angular coefficient functions in (8) for the SM and NP at the benchmark point, using the form factors in Ref. [82]. The bandwidths are due to the uncertainty in the set of form factors.

pseudoscalar and scalar operators in the effective Hamiltonian gives $R_\pi \in [0.5, 1.2]$ [49].

V. REMARKS ABOUT THE MODE $\bar{B} \rightarrow a_1(1260)\ell^-\bar{\nu}_\ell$

As for $\bar{B} \rightarrow \rho(\pi\pi)\ell^-\bar{\nu}_\ell$, the channel $\bar{B} \rightarrow a_1(\rho\pi)\ell^-\bar{\nu}_\ell$ can be numerically analyzed in the SM and in the NP extension (1) using the same benchmark points for the couplings $\epsilon_{V,S,T}^\ell$ and the expressions for the angular coefficient functions in terms of the form factors. Exclusive hadronic B decays into $a_1(1260)$ have been analyzed at the B factories considering the dominant $a_1 \rightarrow \rho\pi$ mode. In particular, $B^0 \rightarrow a_1(1260)^\pm\pi^\mp$ have been scrutinized by the *BABAR* and *Belle* collaborations to carry out measurements of CP violation [72–74].

Observation and measurements of the semileptonic $\bar{B} \rightarrow a_1$ mode are within the present experimental reach, in particular at *Belle II*. The theoretical study of $\bar{B} \rightarrow a_1\ell^-\bar{\nu}_\ell$ requires an assessment of the accuracy of the hadronic quantities. The $\bar{B} \rightarrow a_1$ form factors have been evaluated by different methods [75–84], but a comparative evaluation

of the uncertainties has not been done so far. To present numerical examples, we use the set of form factors in Ref. [82], for which the uncertainty of about 20% is quoted. The angular coefficient functions, for the μ and τ modes and for both the ρ polarizations, are depicted in Figs. 17, 18, 19, and 20. In general, the hadronic uncertainties obscure the effects of the NP operators, confirming the necessity of more precise determinations. Nevertheless, there are coefficient functions in which deviations from SM can be observed, namely, $I_{2s,\parallel}^{a_1}(q^2)$, $I_{6c,\parallel}^{a_1}(q^2)$ (Fig. 17) and $I_{2c,\perp}^{a_1}(q^2)$ (Fig. 19) for the μ channel and $I_{1s,\parallel}^{a_1}(q^2)$, $I_{6s,\parallel}^{a_1}(q^2)$ (Fig. 18) and $I_{1c,\perp}^{a_1}(q^2)$, $I_{6c,\perp}^{a_1}(q^2)$ (Fig. 20) for the τ mode. On the other hand, the forward/backward lepton asymmetry shows sizeable deviations from SM in the case of τ , as shown in Fig. 21.

In the ratio $R_{a_1} = \frac{\mathcal{B}(\bar{B} \rightarrow a_1\tau^-\bar{\nu}_\tau)}{\mathcal{B}(\bar{B} \rightarrow a_1\ell^-\bar{\nu}_\ell)}$, the form factor uncertainty is mild. We obtain, in the SM and for NP at the benchmark point,

$$R_{a_1}^{\text{SM}} = 0.44 \pm 0.07, \quad R_{a_1}^{\text{NP}} = 0.67 \pm 0.12. \quad (24)$$

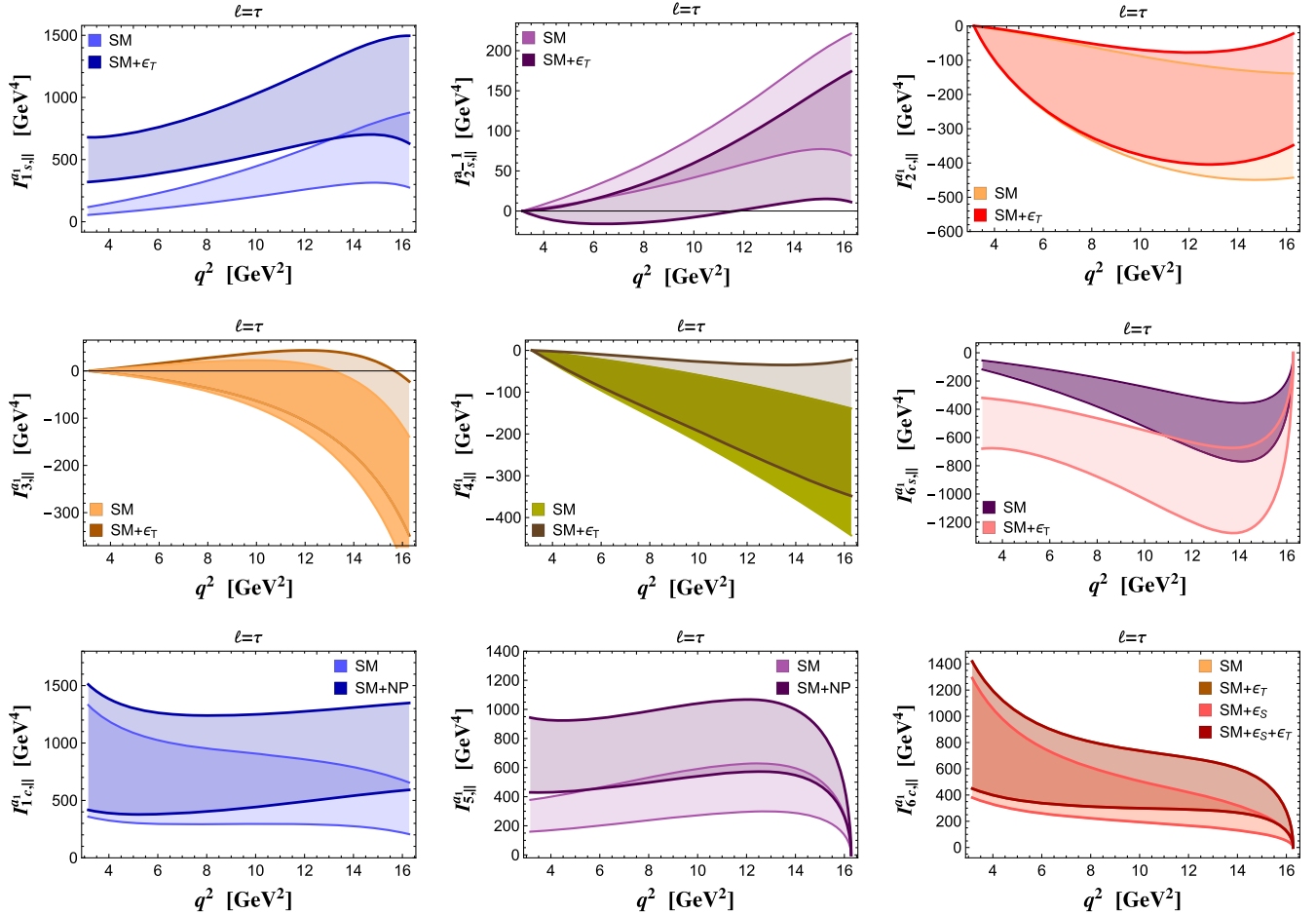


FIG. 18. $\bar{B} \rightarrow a_1(\rho|\pi)\tau^-\bar{\nu}_\tau$ mode, angular coefficient functions with the same notations as in Fig. 17.

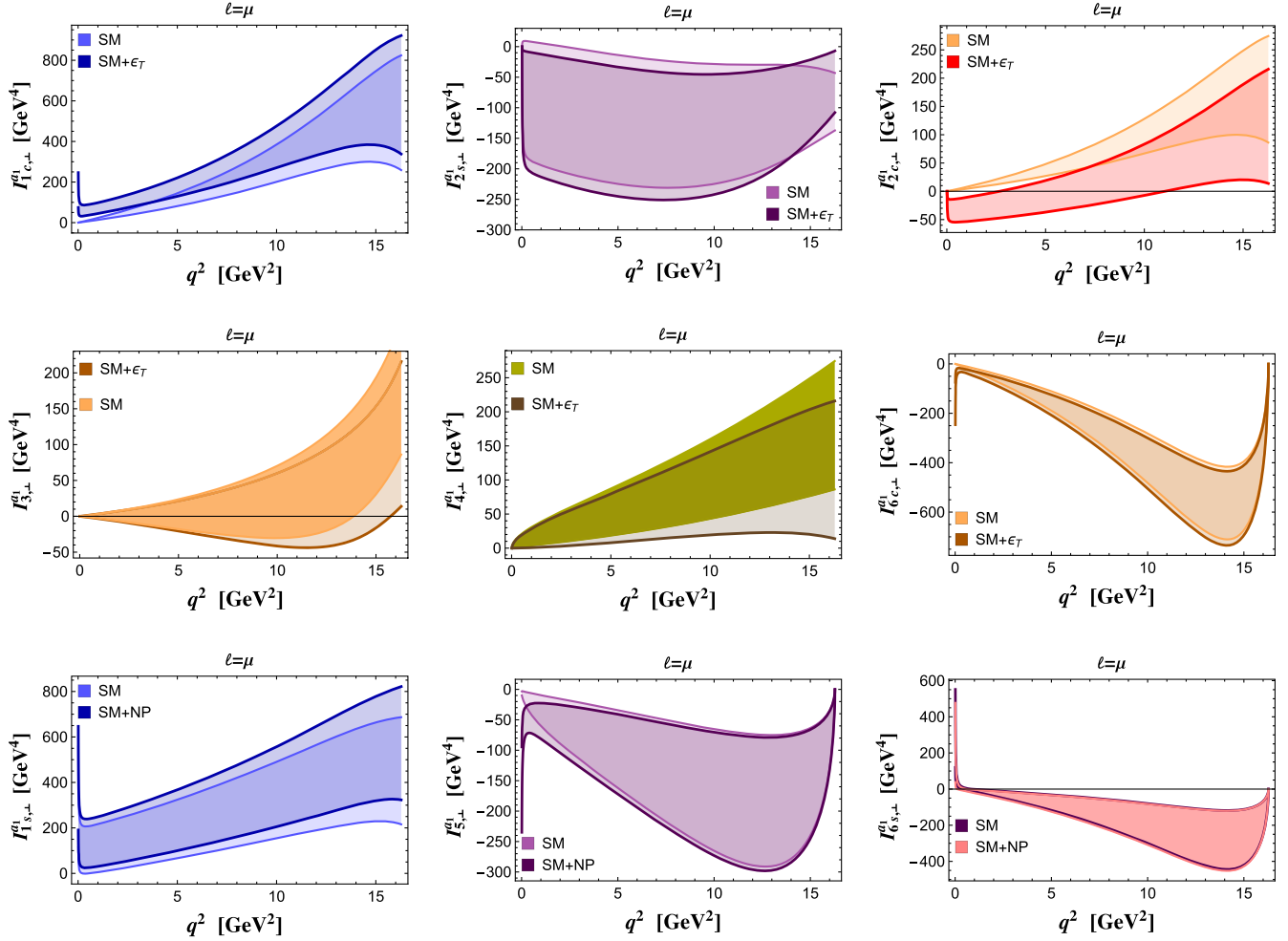


FIG. 19. $\bar{B} \rightarrow a_1(\rho_\perp \pi) \mu^- \bar{\nu}_\mu$ mode, angular coefficient functions with the same notations as in Fig. 17.

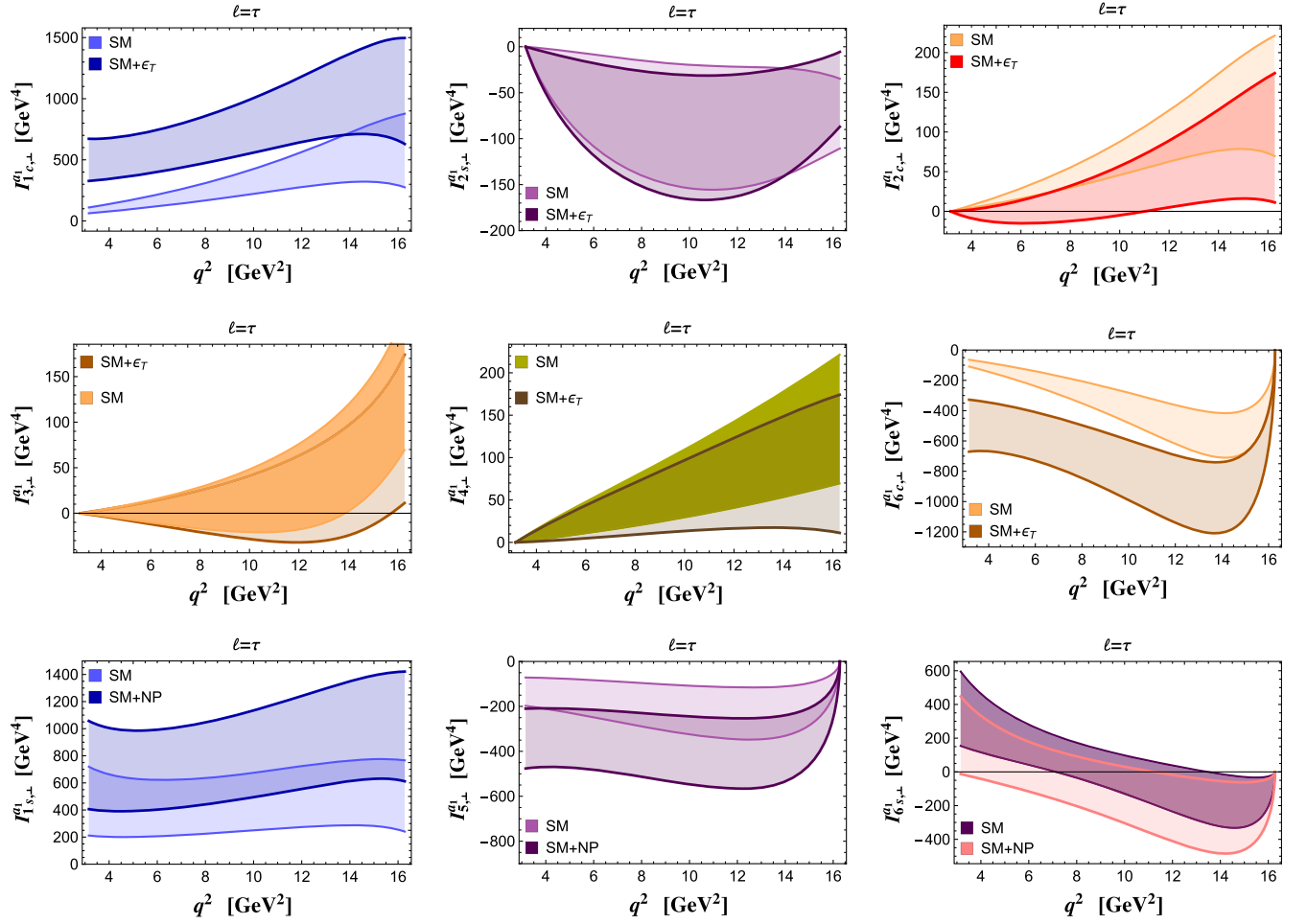
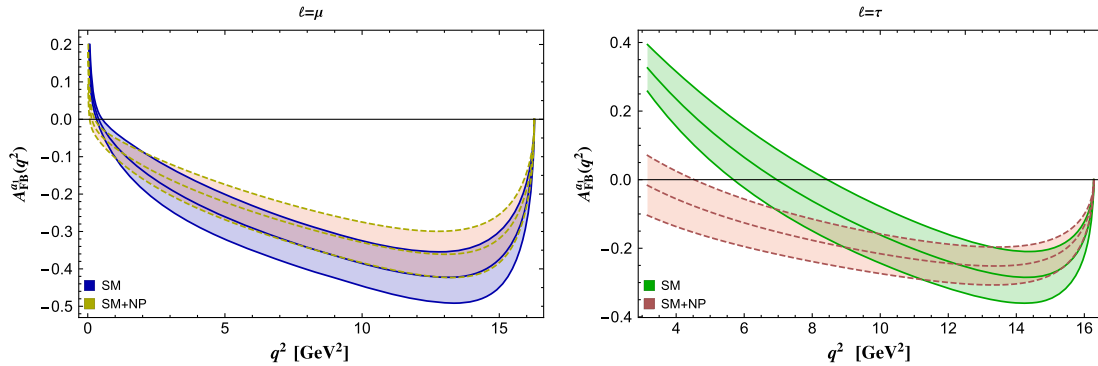
The individual branching fractions in the SM, in this model of form factors, are $\mathcal{B}(\bar{B} \rightarrow a_1^- \mu^- \bar{\nu}_\mu) = (3.0 \pm 1.7) \times 10^{-4}$ and $\mathcal{B}(\bar{B} \rightarrow a_1^- \tau^- \bar{\nu}_\tau) = (1.3 \pm 0.6) \times 10^{-4}$ [82].

We can now summarize the synergies between the various considered modes to provide possible evidences of NP in semileptonic $b \rightarrow u$ transitions:

- (i) The presence of the tensor structure in the effective Hamiltonian can be established independently of the presence of the other operators, looking at deviations of the observables that depend only on ϵ_T . These are the observables involving transversely polarized ρ and a_1 . Moreover, it is possible to tightly constrain $|\epsilon_T|$ looking at the zero of the ratios defined in Eqs. (11) and (12). A correlation between the position of the zero in the ρ and a_1 modes should be observed, as in Fig. 10.
- (ii) If a pseudoscalar operator is present, without other NP structures, deviations should be observed in leptonic B decays and in the semileptonic decay to ρ , not in semileptonic decays to π and a_1 . Determining the position of the zero in I_{6c}^ρ allows

us to constrain $\text{Re}[\epsilon_P]$. Zeros should not be present in $I_{6c,||}^{a_1}$.

- (iii) If a scalar operator is present, without additional NP structures, deviations should be observed in semi-leptonic B decays to π and a_1 . In particular, a zero would be present in $I_{6c,||}^{a_1}$, not in I_{6c}^ρ .
- (iv) The simultaneous presence of all the operators would manifest in a more involved pattern of deviations. However, such deviations are correlated in the two modes, and the pattern of correlation can be used to assess the role of the various new terms in (1).
- (v) Precise measurements of modes with final τ provide new important tests of LFU. The determination of R_ρ and R_π would give information on the relative sign of $\text{Re}[\epsilon_T^\mu]$ and $\text{Re}[\epsilon_T^\tau]$, as shown in Fig. 16. In the a_1 channel, deviations are also expected. However, in this case, the reconstruction of the modes with τ is challenging; for example, using the three prong channel for the τ reconstruction implies considering a final state comprising six light mesons.


 FIG. 20. $\bar{B} \rightarrow a_1(\rho_\perp \pi) \tau^- \bar{\nu}_\tau$ mode, angular coefficient functions with the same notations as in Fig. 17.

 FIG. 21. $\bar{B} \rightarrow a_1 \ell^- \bar{\nu}_\ell$ mode: FB lepton asymmetries for $\ell = \mu$ (left) and τ (right).

VI. CONCLUSIONS

The questions raised by the anomalies in $b \rightarrow c$ semileptonic modes call for new analyses on the CKM suppressed semileptonic $b \rightarrow u$ modes, for which precise measurements are expected. We have considered an enlarged SM effective Hamiltonian including additional $D = 6$ operators and looked for the impact of the new terms

on $\bar{B} \rightarrow \rho(\pi\pi)\ell^- \bar{\nu}_\ell$ and $\bar{B} \rightarrow a_1(\rho\pi)\ell^- \bar{\nu}_\ell$. We have constructed the four-dimensional differential distribution for both the modes, finding that they are sensitive to different NP operators. The different quantum numbers of light mesons in the two processes act as a selection on the contributions of the NP terms; therefore, the two modes provide complementary information about the role of the

new operators in Eq. (1). This motivates their consideration. We have constrained the parameter space of the effective coupling constants from current data on purely leptonic and semileptonic B modes into a pseudoscalar meson and considered the impact on $\bar{B} \rightarrow \rho \ell^- \bar{\nu}_\ell$. Among the various observables, we have found that a few angular coefficients present zeros that do not appear in the SM, the observation of which would represent support toward the confirmation of NP effects. We have defined integrated decay distributions, useful for comparing the modes into μ and τ , with the aim of further testing LFU. In the perspective of precision analyses, the theoretical error connected to the hadronic matrix elements represents a sizable uncertainty needing to be reduced, in particular for the a_1 mode. The combination of different determinations based on QCD (QCD sum rules and lattice QCD), obtained

in their respective domains of validity, can be a strategy for reducing the theoretical uncertainty. The large energy limit, in which the number of hadronic form factors is reduced, also represents a way to analyze these two modes. The possibility of finding deviations from the SM fully justifies the careful scrutiny of such promising processes.

ACKNOWLEDGMENTS

This study has been carried out within the INFN project (Iniziativa Specifica) QFT-HEP.

APPENDIX A: HADRONIC MATRIX ELEMENTS

For the $M_u = \pi^+$ meson, the weak matrix elements are written in terms of form factors as follows,

$$\begin{aligned}
\langle \pi(p') | \bar{u} \gamma_\mu b | \bar{B}(p) \rangle &= f_+^{B \rightarrow \pi}(q^2) \left[p_\mu + p'_\mu - \frac{m_B^2 - m_\pi^2}{q^2} q_\mu \right] + f_0^{B \rightarrow \pi}(q^2) \frac{m_B^2 - m_\pi^2}{q^2} q_\mu \\
\langle \pi(p') | \bar{u} b | \bar{B}(p) \rangle &= f_S^{B \rightarrow \pi}(q^2) \\
\langle \pi(p') | \bar{u} \sigma_{\mu\nu} b | \bar{B}(p) \rangle &= -i \frac{2f_T^{B \rightarrow \pi}(q^2)}{m_B + m_\pi} [p_\mu p'_\nu - p_\nu p'_\mu] \\
\langle \pi(p') | \bar{u} \sigma_{\mu\nu} \gamma_5 b | \bar{B}(p) \rangle &= -\frac{2f_T^{B \rightarrow \pi}(q^2)}{m_B + m_\pi} \epsilon_{\mu\nu\alpha\beta} p^\alpha p'^\beta,
\end{aligned} \tag{A1}$$

where $\epsilon^{0123} = +1$. The relation $f_S^{B \rightarrow \pi}(q^2) = \frac{m_B^2 - m_\pi^2}{m_b - m_u} f_0^{B \rightarrow \pi}(q^2)$ holds.

For $M_u = \rho^+$, the various matrix elements, expressed in terms of form factors (with ϵ the ρ polarization vector), read

$$\begin{aligned}
\langle \rho(p', \epsilon) | \bar{u} \gamma_\mu (1 - \gamma_5) b | \bar{B}(p) \rangle &= -\frac{2V^{B \rightarrow \rho}(q^2)}{m_B + m_\rho} i \epsilon_{\mu\alpha\beta} \epsilon^{*\nu} p^\alpha p'^\beta \\
&\quad - \left\{ (m_B + m_\rho) \left[\epsilon_\mu^* - \frac{(\epsilon^* \cdot q)}{q^2} q_\mu \right] A_1^{B \rightarrow \rho}(q^2) - \frac{(\epsilon^* \cdot q)}{m_B + m_\rho} \left[(p + p')_\mu - \frac{m_B^2 - m_\rho^2}{q^2} q_\mu \right] A_2^{B \rightarrow \rho}(q^2) \right. \\
&\quad \left. + (\epsilon^* \cdot q) \frac{2m_\rho}{q^2} q_\mu A_0^{B \rightarrow \rho}(q^2) \right\},
\end{aligned} \tag{A2}$$

with the condition $A_0^{B \rightarrow \rho}(0) = \frac{m_B + m_\rho}{2m_\rho} A_1^{B \rightarrow \rho}(0) - \frac{m_B - m_\rho}{2m_\rho} A_2^{B \rightarrow \rho}(0)$, and

$$\langle \rho(p', \epsilon) | \bar{u} \gamma_5 b | \bar{B}(p) \rangle = -\frac{2m_\rho}{m_b + m_u} (\epsilon^* \cdot q) A_0^{B \rightarrow \rho}(q^2) \tag{A3}$$

$$\langle \rho(p', \epsilon) | \bar{u} \sigma_{\mu\nu} b | \bar{B}(p) \rangle = T_0^{B \rightarrow \rho}(q^2) \frac{\epsilon^* \cdot q}{(m_B + m_\rho)^2} \epsilon_{\mu\nu\alpha\beta} p^\alpha p'^\beta + T_1^{B \rightarrow \rho}(q^2) \epsilon_{\mu\nu\alpha\beta} p^\alpha \epsilon^{*\beta} + T_2^{B \rightarrow \rho}(q^2) \epsilon_{\mu\nu\alpha\beta} p'^\alpha \epsilon^{*\beta} \tag{A4}$$

$$\begin{aligned}
\langle \rho(p', \epsilon) | \bar{u} \sigma_{\mu\nu} \gamma_5 b | \bar{B}(p) \rangle &= iT_0^{B \rightarrow \rho}(q^2) \frac{\epsilon^* \cdot q}{(m_B + m_\rho)^2} (p_\mu p'_\nu - p_\nu p'_\mu) + iT_1^{B \rightarrow \rho}(q^2) (p_\mu \epsilon_\nu^* - \epsilon_\mu^* p_\nu) \\
&\quad + iT_2^{B \rightarrow \rho}(q^2) (p'_\mu \epsilon_\nu^* - \epsilon_\mu^* p'_\nu).
\end{aligned} \tag{A5}$$

For $M_u = a_1^+$, we use the decomposition:

$$\begin{aligned} \langle a_1(p', \epsilon) | \bar{u} \gamma_\mu (1 - \gamma_5) b | \bar{B}(p) \rangle &= \frac{2A^{B \rightarrow a_1}(q^2)}{m_B + m_{a_1}} i \epsilon_{\mu\nu\alpha\beta} \epsilon^{*\nu} p^\alpha p'^\beta \\ &+ \left\{ (m_B + m_{a_1}) \left[\epsilon_\mu^* - \frac{(\epsilon^* \cdot q)}{q^2} q_\mu \right] V_1^{B \rightarrow a_1}(q^2) \right. \\ &\left. - \frac{(\epsilon^* \cdot q)}{m_B + m_{a_1}} \left[(p + p')_\mu - \frac{m_B^2 - m_{a_1}^2}{q^2} q_\mu \right] V_2^{B \rightarrow a_1}(q^2) + (\epsilon^* \cdot q) \frac{2m_{a_1}}{q^2} q_\mu V_0^{B \rightarrow a_1}(q^2) \right\} \end{aligned} \quad (\text{A6})$$

with the condition $V_0^{B \rightarrow a_1}(0) = \frac{m_B + m_{a_1}}{2m_{a_1}} V_1^{B \rightarrow a_1}(0) - \frac{m_B - m_{a_1}}{2m_{a_1}} V_2^{B \rightarrow a_1}(0)$, and

$$\langle a_1(p', \epsilon) | \bar{u} b | \bar{B}(p) \rangle = \frac{2m_{a_1}}{m_b - m_u} (\epsilon^* \cdot q) V_0^{B \rightarrow a_1}(q^2) \quad (\text{A7})$$

$$\begin{aligned} \langle a_1(p', \epsilon) | \bar{u} \sigma_{\mu\nu} b | \bar{B}(p) \rangle &= iT_0^{B \rightarrow a_1}(q^2) \frac{\epsilon^* \cdot q}{(m_B + m_{a_1})^2} (p_\mu p'_\nu - p_\nu p'_\mu) \\ &+ iT_1^{B \rightarrow a_1}(q^2) (p_\mu \epsilon_\nu^* - \epsilon_\mu^* p_\nu) + iT_2^{B \rightarrow a_1}(q^2) (p'_\mu \epsilon_\nu^* - \epsilon_\mu^* p'_\nu) \end{aligned} \quad (\text{A8})$$

$$\begin{aligned} \langle a_1(p', \epsilon) | \bar{u} \sigma_{\mu\nu} \gamma_5 b | \bar{B}(p) \rangle &= T_0^{B \rightarrow a_1}(q^2) \frac{\epsilon^* \cdot q}{(m_B + m_{a_1})^2} \epsilon_{\mu\nu\alpha\beta} p^\alpha p'^\beta \\ &+ T_1^{B \rightarrow a_1}(q^2) \epsilon_{\mu\nu\alpha\beta} p^\alpha \epsilon^{*\beta} + T_2^{B \rightarrow a_1}(q^2) \epsilon_{\mu\nu\alpha\beta} p'^\alpha \epsilon^{*\beta}. \end{aligned} \quad (\text{A9})$$

In the large energy (large recoil) limit for the light meson, the weak matrix elements can be expressed in terms of a smaller number of form factors. We define $E = \frac{m_b^2 + m^2 - q^2}{2m_b}$ as the light meson energy in the B rest frame and m as the light meson mass. The B 4-velocity is defined from $p = m_B v$, and n_- is a lightlike 4-vector along p' : $p' = E n_-$. In the large recoil configuration, for $E \simeq \frac{m_b}{2}$, the light quark u carries almost all the momentum of the light meson, $p'_{u\mu} = E(n_-)_\mu + k_\mu$, with the residual momentum $k \ll E$. Using, e.g., an eikonal formulation of the weak current, this allows us to express the form factors in terms

of universal functions $\xi_i(E)$ [50,51]. For $B \rightarrow \pi$, a single form factor $\xi_\pi(E)$ parametrizes the matrix elements,

$$\begin{aligned} \langle \pi(p') | \bar{u} \gamma_\mu b | \bar{B}(p) \rangle &= 2E \xi_\pi(E) (n_-)_\mu \\ \langle \pi(p') | \bar{u} \sigma_{\mu\nu} q^\nu b | \bar{B}(p) \rangle &= 2iE \xi_\pi(E) [(m_B - E)(n_-)_\mu - m_B v_\mu]. \end{aligned} \quad (\text{A10})$$

For $B \rightarrow \rho$, there are two independent form factors, $\xi_\perp^\rho(E)$ and $\xi_\parallel^\rho(E)$,

$$\begin{aligned} \langle \rho(p', \epsilon) | \bar{u} \gamma_\mu b | \bar{B}(p) \rangle &= 2iE \xi_\perp^\rho(E) \epsilon_{\mu\nu\alpha\beta} \epsilon^{*\nu} (n_-)^\alpha v^\beta \\ \langle \rho(p', \epsilon) | \bar{u} \gamma_\mu \gamma_5 b | \bar{B}(p) \rangle &= 2E \{ \xi_\perp^\rho(E) [\epsilon_\mu^* - (\epsilon^* \cdot v)(n_-)_\mu] + \xi_\parallel^\rho(E) (\epsilon^* \cdot v)(n_-)_\mu \} \\ \langle \rho(p', \epsilon) | \bar{u} \sigma_{\mu\nu} q^\nu b | \bar{B}(p) \rangle &= 2Em_B \xi_\perp^\rho(E) \epsilon_{\mu\nu\alpha\beta} \epsilon^{*\nu} v^\alpha (n_-)^\beta \\ \langle \rho(p', \epsilon) | \bar{u} \sigma_{\mu\nu} \gamma_5 q^\nu b | \bar{B}(p) \rangle &= -2iE \{ \xi_\perp^\rho(E) m_B [\epsilon_\mu^* - (\epsilon^* \cdot v)(n_-)_\mu] + \xi_\parallel^\rho(E) (\epsilon^* \cdot v) [(m_B - E)(n_-)_\mu - m_B v_\mu] \}, \end{aligned} \quad (\text{A11})$$

and two independent $\xi_\perp^{a_1}(E)$ and $\xi_\parallel^{a_1}(E)$ for factors are also involved for a_1 ,

$$\begin{aligned} \langle a_1(p', \epsilon) | \bar{u} \gamma_\mu \gamma_5 b | \bar{B}(p) \rangle &= -2iE \xi_\perp^{a_1}(E) \epsilon_{\mu\nu\alpha\beta} \epsilon^{*\nu} (n_-)^\alpha v^\beta \\ \langle a_1(p', \epsilon) | \bar{u} \gamma_\mu b | \bar{B}(p) \rangle &= -2E \{ \xi_\perp^{a_1}(E) [\epsilon_\mu^* - (\epsilon^* \cdot v)(n_-)_\mu] + \xi_\parallel^{a_1}(E) (\epsilon^* \cdot v)(n_-)_\mu \} \\ \langle a_1(p', \epsilon) | \bar{u} \sigma_{\mu\nu} q^\nu \gamma_5 b | \bar{B}(p) \rangle &= 2Em_B \xi_\perp^{a_1}(E) \epsilon_{\mu\nu\alpha\beta} \epsilon^{*\nu} v^\alpha (n_-)^\beta \\ \langle a_1(p', \epsilon) | \bar{u} \sigma_{\mu\nu} q^\nu b | \bar{B}(p) \rangle &= -2iE \{ \xi_\perp^{a_1}(E) m_B [\epsilon_\mu^* - (\epsilon^* \cdot v)(n_-)_\mu] + \xi_\parallel^{a_1}(E) (\epsilon^* \cdot v) [(m_B - E)(n_-)_\mu - m_B v_\mu] \}. \end{aligned} \quad (\text{A12})$$

Comparing Eqs. (A1)–(A8) with Eqs. (A10)–(A12), the relations among the form factors and their large energy limit expressions can be worked out. For $B \rightarrow \pi$, they are

$$\begin{aligned} f_+^{B \rightarrow \pi}(q^2) &= \frac{m_B}{2E} f_0^{B \rightarrow \pi}(q^2) = \frac{m_B}{m_B + m_\pi} f_T^{B \rightarrow \pi}(q^2) \\ &= \xi_\pi(E); \end{aligned} \quad (\text{A13})$$

for $B \rightarrow \rho$, they are

$$\begin{aligned} \frac{m_B}{m_B + m_\rho} V^{B \rightarrow \rho}(q^2) &= \frac{m_B + m_\rho}{2E} A_1^{B \rightarrow \rho}(q^2) = \xi_\perp^\rho(E) \\ \frac{m_\rho}{E} A_0^{B \rightarrow \rho}(q^2) &= \frac{m_B + m_\rho}{2E} A_1^{B \rightarrow \rho}(q^2) \\ &\quad - \frac{m_B - m_\rho}{m_B} A_2^{B \rightarrow \rho}(q^2) = \xi_{||}^\rho(E) \\ T_1^{B \rightarrow \rho}(q^2) &= 0 \\ T_2^{B \rightarrow \rho}(q^2) &= 2\xi_\perp^\rho(E) \\ T_0^{B \rightarrow \rho}(q^2) &= 2\xi_{||}^\rho(E); \end{aligned} \quad (\text{A14})$$

and for $B \rightarrow a_1$, they are

$$\begin{aligned} \frac{m_B}{m_B + m_{a_1}} A^{B \rightarrow a_1}(q^2) &= \frac{m_B + m_{a_1}}{2E} V_1^{B \rightarrow a_1}(q^2) = \xi_\perp^{a_1}(E) \\ \frac{m_{a_1}}{E} V_0^{B \rightarrow a_1}(q^2) &= \frac{m_B + m_{a_1}}{2E} V_1^{B \rightarrow a_1}(q^2) \\ &\quad - \frac{m_B - m_{a_1}}{m_B} V_2^{B \rightarrow a_1}(q^2) = \xi_{||}^{a_1}(E) \\ T_1^{B \rightarrow a_1}(q^2) &= 0 \\ T_2^{B \rightarrow a_1}(q^2) &= 2\xi_\perp^{a_1}(E) \\ T_0^{B \rightarrow a_1}(q^2) &= 2\xi_{||}^{a_1}(E). \end{aligned} \quad (\text{A15})$$

The functions ξ_π , $\xi_{||}^\rho$, and ξ_\perp^ρ have been determined by light-cone QCD sum rules within the Soft Collinear Effective Theory, using B meson light-cone distribution amplitudes [85–87].

APPENDIX B: ANGULAR COEFFICIENT FUNCTIONS

Here, we collect the expressions of the angular coefficient functions in Eqs. (7) and (8). The general form of the $\bar{B} \rightarrow V\ell^-\bar{\nu}_\ell$ decay amplitude, with $V = \rho$ and a_1 ,

$$\begin{aligned} \mathcal{A}(\bar{B} \rightarrow V\ell^-\bar{\nu}_\ell) &= \frac{G_F}{\sqrt{2}} V_{ub} [(1 + \epsilon_V^\ell) H_\mu^{\text{SM}} L^{\text{SM}\mu} \\ &\quad + \epsilon_S^\ell H^{\text{NP},S} L^{\text{NP},S} + \epsilon_P^\ell H^{\text{NP},P} L^{\text{NP},P} \\ &\quad + \epsilon_T^\ell H_{\mu\nu}^{\text{NP},T} L^{\text{NP},T\mu\nu}], \end{aligned} \quad (\text{B1})$$

is given in terms of the quark current matrix elements

$$\begin{aligned} H_\mu^{\text{SM}}(m) &= \langle V(p_V, \epsilon(m)) | \bar{u}\gamma_\mu(1 - \gamma_5)b | \bar{B}(p_B) \rangle \\ &= \epsilon^{*\alpha}(m) T_{\mu\alpha} \end{aligned} \quad (\text{B2})$$

$$H^{\text{NP},S}(m) = \langle V(p_V, \epsilon(m)) | \bar{u}b | \bar{B}(p_B) \rangle = \epsilon^{*\alpha}(m) T_\alpha^{\text{NP},S} \quad (\text{B3})$$

$$H_\mu^{\text{NP},P}(m) = \langle V(p_V, \epsilon(m)) | \bar{u}\gamma_5b | \bar{B}(p_B) \rangle = \epsilon^{*\alpha}(m) T_\alpha^{\text{NP},P} \quad (\text{B4})$$

$$\begin{aligned} H_{\mu\nu}^{\text{NP},T}(m) &= \langle D^*(p_{D^*}, \epsilon(m)) | \bar{c}\sigma_{\mu\nu}(1 - \gamma_5)b | \bar{B}(p_B) \rangle \\ &= \epsilon^{*\alpha}(m) T_{\mu\nu\alpha}^{\text{NP},T} \end{aligned} \quad (\text{B5})$$

and of the lepton currents

$$L^{\text{SM}\mu} = \bar{\ell}\gamma^\mu(1 - \gamma_5)\nu_\ell \quad (\text{B6})$$

$$L^{\text{NP},S} = L^{\text{NP},P} = \bar{\ell}(1 - \gamma_5)\nu_\ell \quad (\text{B7})$$

$$L^{\text{NP},T\mu\nu} = \bar{\ell}\sigma^{\mu\nu}(1 - \gamma_5)\nu_\ell. \quad (\text{B8})$$

In the SM, one can relate the helicity amplitudes for the V polarization states to the polarizations of the virtual $W(q, \bar{\epsilon})$. In the lepton pair rest frame, they are

$$\bar{\epsilon}_\pm = \frac{1}{\sqrt{2}}(0, 1, \pm i, 0), \quad \bar{\epsilon}_0 = (0, 0, 0, 1), \quad \bar{\epsilon}_t = (1, 0, 0, 0). \quad (\text{B9})$$

This allows us to define the amplitudes

$$\begin{aligned} H_m &= \bar{\epsilon}_m^{*\mu} \epsilon_m^{*\alpha} T_{\mu\alpha} \quad (m = 0, \pm) \\ H_t &= \bar{\epsilon}_t^{*\mu} \epsilon_0^{*\alpha} T_{\mu\alpha} \quad (m = t), \end{aligned} \quad (\text{B10})$$

which can be expressed in terms of the form factors in (A2) and (A6),

$$\begin{aligned} H_0^\rho &= \frac{(m_B + m_\rho)^2(m_B^2 - m_\rho^2 - q^2)A_1(q^2) - \lambda(m_B^2, m_\rho^2, q^2)A_2(q^2)}{2m_\rho(m_B + m_\rho)\sqrt{q^2}} \\ H_\pm^\rho &= \frac{(m_B + m_\rho)^2A_1(q^2) \mp \sqrt{\lambda(m_B^2, m_\rho^2, q^2)}V(q^2)}{m_B + m_\rho} \\ H_t^\rho &= -\frac{\sqrt{\lambda(m_B^2, m_\rho^2, q^2)}}{\sqrt{q^2}}A_0(q^2) \end{aligned} \quad (\text{B11})$$

and

$$\begin{aligned}
 H_0^{a_1} &= \frac{-(m_B + m_{a_1})^2(m_B^2 - m_{a_1}^2 - q^2)V_1(q^2) + \lambda(m_B^2, m_{a_1}^2, q^2)V_2(q^2)}{2m_{a_1}(m_B + m_{a_1})\sqrt{q^2}} \\
 H_{\pm}^{a_1} &= \frac{-(m_B + m_{a_1})^2V_1(q^2) \pm \sqrt{\lambda(m_B^2, m_{a_1}^2, q^2)}A(q^2)}{m_B + m_{a_1}} \\
 H_t^{a_1} &= \frac{\sqrt{\lambda(m_B^2, m_{a_1}^2, q^2)}}{\sqrt{q^2}}V_0(q^2).
 \end{aligned} \tag{B12}$$

No new definitions are needed in the case of S and P operators, since their matrix elements involve the same form factors as in the SM. For the NP tensor operator, one defines [32]

$$\begin{aligned}
 H_+^{\text{NP},\rho} &= \frac{1}{\sqrt{q^2}} \{ [m_B^2 - m_\rho^2 + \lambda^{1/2}(m_B^2, m_\rho^2, q^2)](T_1^{B \rightarrow \rho} + T_2^{B \rightarrow \rho}) + q^2(T_1^{B \rightarrow \rho} - T_2^{B \rightarrow \rho}) \} \\
 H_-^{\text{NP},\rho} &= \frac{1}{\sqrt{q^2}} \{ [m_B^2 - m_\rho^2 - \lambda^{1/2}(m_B^2, m_\rho^2, q^2)](T_1^{B \rightarrow \rho} + T_2^{B \rightarrow \rho}) + q^2(T_1^{B \rightarrow \rho} - T_2^{B \rightarrow \rho}) \} \\
 H_L^{\text{NP},\rho} &= 4 \left\{ \frac{\lambda(m_B^2, m_\rho^2, q^2)}{m_\rho(m_B + m_\rho)^2} T_0^{B \rightarrow \rho} + 2 \frac{m_B^2 + m_\rho^2 - q^2}{m_\rho} T_1^{B \rightarrow \rho} + 4m_\rho T_2^{B \rightarrow \rho} \right\}.
 \end{aligned} \tag{B13}$$

The expressions for $H_{(+,-,L)}^{\text{NP},a_1}$ are obtained by replacing $m_\rho \rightarrow m_{a_1}$ and $T_i^{B \rightarrow \rho} \rightarrow T_i^{B \rightarrow a_1}$.

For the decay $\bar{B} \rightarrow a_1(\rho\pi)\ell^-\bar{\nu}_\ell$, we define the ρ helicity amplitudes $\mathcal{A}_1, \mathcal{A}_{-1}, \mathcal{A}_0$ for $\lambda = +1, -1, 0$. Writing the matrix element

$$\begin{aligned}
 \langle \rho(p_\rho, \eta)\pi(p_\pi) | a_1(p', \epsilon) \rangle &= g_1(\epsilon \cdot \eta^*)(p' \cdot p_\rho) \\
 &+ g_2(\epsilon \cdot p_\rho)(p' \cdot \eta^*)
 \end{aligned} \tag{B14}$$

in terms of the couplings g_1 and g_2 , we have

TABLE II. Angular coefficient functions in the four-dimensional $\bar{B} \rightarrow \rho(\pi\pi)\ell^-\bar{\nu}_\ell$ decay distribution, Eq. (7), in the SM.

i	I_i^{SM}
I_{1s}^ρ	$\frac{1}{2}(H_+^2 + H_-^2)(m_\ell^2 + 3q^2)$
I_{1c}^ρ	$4m_\ell^2 H_t^2 + 2H_0^2(m_\ell^2 + q^2)$
I_{2s}^ρ	$-\frac{1}{2}(H_+^2 + H_-^2)(m_\ell^2 - q^2)$
I_{2c}^ρ	$2H_0^2(m_\ell^2 - q^2)$
I_3^ρ	$2H_+H_-(m_\ell^2 - q^2)$
I_4^ρ	$H_0(H_+ + H_-)(m_\ell^2 - q^2)$
I_5^ρ	$-2H_t(H_+ + H_-)m_\ell^2 - 2H_0(H_+ - H_-)q^2$
I_{6s}^ρ	$2(H_+^2 - H_-^2)q^2$
I_{6c}^ρ	$-8H_tH_0m_\ell^2$
I_7^ρ	0

$$\Gamma(a_1 \rightarrow \rho\pi) = \frac{|\vec{p}_\rho|}{24\pi m_{a_1}^2} (\tilde{\Gamma}_\perp + \tilde{\Gamma}_\parallel), \tag{B15}$$

where $|\vec{p}_\rho| = \frac{\lambda^{1/2}(m_{a_1}^2, m_\rho^2, m_\pi^2)}{2m_{a_1}}$ and

$$\begin{aligned}
 \tilde{\Gamma}_\perp &= 2|\mathcal{A}_1|^2 = 2g_1^2 m_{a_1}^2 (m_\rho^2 + |\vec{p}_\rho|^2) \\
 \tilde{\Gamma}_\parallel &= |\mathcal{A}_0|^2 = \frac{m_{a_1}^2}{m_\rho^2} [(m_\rho^2 + |\vec{p}_\rho|^2)g_1 + |\vec{p}_\rho|^2 g_2]^2.
 \end{aligned} \tag{B16}$$

The branching ratios for ρ longitudinally and transversely polarized, appearing in the factors $\mathcal{N}_{a_1}^{||(\perp)}$ in Eq. (8), read

$$\mathcal{B}(a_1 \rightarrow \rho_{||(\perp)}\pi) = \frac{1}{\Gamma(a_1)} \frac{|\vec{p}_\rho|}{24\pi m_{a_1}^2} \tilde{\Gamma}_{||(\perp)}. \tag{B17}$$

APPENDIX C: $B \rightarrow \pi$ FORM FACTORS AND OTHER PARAMETERS

For the $B \rightarrow \pi$ form factors defined in (A1), we use the parametrization [88]

TABLE III. Angular coefficient functions for $\bar{B} \rightarrow \rho(\pi\pi)\ell^-\bar{\nu}_\ell$: NP term with P operator, interference term SM-NP with P operator, and NP-NP interference terms between P and T operators, Eq. (9).

i	$I_i^{\text{NP},P}$	$I_i^{\text{INT},P}$	$I_i^{\text{INT},PT}$
I_{1s}^ρ	0	0	0
I_{1c}^ρ	$4H_t^2 \frac{q^4}{(m_b+m_u)^2}$	$4H_t^2 \frac{m_\ell q^2}{m_b+m_u}$	0
I_{2s}^ρ	0	0	0
I_{2c}^ρ	0	0	0
I_3^ρ	0	0	0
I_4^ρ	0	0	0
I_5^ρ	0	$-H_t(H_+ + H_-) \frac{m_\ell q^2}{m_b+m_u}$	$2H_t(H_+^{\text{NP}} + H_-^{\text{NP}}) \frac{(q^2)^{3/2}}{m_b+m_u}$
I_{6s}^ρ	0	0	0
I_{6c}^ρ	0	$-4H_t H_0 \frac{m_\ell q^2}{m_b+m_u}$	$H_t H_L^{\text{NP}} \frac{(q^2)^{3/2}}{m_b+m_u}$
I_7^ρ	0	$-H_t(H_+ - H_-) \frac{m_\ell q^2}{m_b+m_u}$	$2H_t(H_+^{\text{NP}} - H_-^{\text{NP}}) \frac{(q^2)^{3/2}}{m_b+m_u}$

TABLE IV. Angular coefficient functions for $\bar{B} \rightarrow \rho(\pi\pi)\ell^-\bar{\nu}_\ell$: NP term with T operator and interference term SM-NP with T operator, Eq. (9).

i	$I_i^{\text{NP},T}$	$I_i^{\text{INT},T}$
I_{1s}^ρ	$2[(H_+^{\text{NP}})^2 + (H_-^{\text{NP}})^2](3m_\ell^2 + q^2)$	$-4(H_+^{\text{NP}}H_+ + H_-^{\text{NP}}H_-)m_\ell\sqrt{q^2}$
I_{1c}^ρ	$\frac{1}{8}(H_L^{\text{NP}})^2(m_\ell^2 + q^2)$	$-H_L^{\text{NP}}H_0m_\ell\sqrt{q^2}$
I_{2s}^ρ	$2[(H_+^{\text{NP}})^2 + (H_-^{\text{NP}})^2](m_\ell^2 - q^2)$	0
I_{2c}^ρ	$\frac{1}{8}(H_L^{\text{NP}})^2(q^2 - m_\ell^2)$	0
I_3^ρ	$8H_+^{\text{NP}}H_-^{\text{NP}}(q^2 - m_\ell^2)$	0
I_4^ρ	$\frac{1}{2}H_L^{\text{NP}}(H_+^{\text{NP}} + H_-^{\text{NP}})(q^2 - m_\ell^2)$	0
I_5^ρ	$-H_L^{\text{NP}}(H_+^{\text{NP}} - H_-^{\text{NP}})m_\ell^2$	$\frac{1}{4}[H_L^{\text{NP}}(H_+ - H_-) + 8H_+^{\text{NP}}(H_t + H_0) + 8H_-^{\text{NP}}(H_t - H_0)]m_\ell\sqrt{q^2}$
I_{6s}^ρ	$8[(H_+^{\text{NP}})^2 - (H_-^{\text{NP}})^2]m_\ell^2$	$-4(H_+^{\text{NP}}H_+ - H_-^{\text{NP}}H_-)m_\ell\sqrt{q^2}$
I_{6c}^ρ	0	$H_L^{\text{NP}}H_t m_\ell\sqrt{q^2}$
I_7^ρ	0	$\frac{1}{4}[H_L^{\text{NP}}(H_+ + H_-) - 8H_+^{\text{NP}}(H_t + H_0) + 8H_-^{\text{NP}}(H_t - H_0)]m_\ell\sqrt{q^2}$

TABLE V. Angular coefficient functions in the four-dimensional $\bar{B} \rightarrow a_1(\rho\pi)\ell^-\bar{\nu}_\ell$ decay distribution, Eq. (8), in the SM.

i	$I_{i,\parallel}^{\text{SM}}$	$I_{i,\perp}^{\text{SM}}$
$I_{1s}^{a_1}$	$\frac{1}{2}(H_+^2 + H_-^2)(m_\ell^2 + 3q^2)$	$2H_t^2 m_\ell^2 + H_0^2(m_\ell^2 + q^2) + \frac{1}{4}(H_+^2 + H_-^2)(m_\ell^2 + 3q^2)$
$I_{1c}^{a_1}$	$4H_t^2 m_\ell^2 + 2H_0^2(m_\ell^2 + q^2)$	$\frac{1}{2}(H_+^2 + H_-^2)(m_\ell^2 + 3q^2)$
$I_{2s}^{a_1}$	$-\frac{1}{2}(H_+^2 + H_-^2)(m_\ell^2 - q^2)$	$[H_0^2 - \frac{1}{4}(H_+^2 + H_-^2)](m_\ell^2 - q^2)$
$I_{2c}^{a_1}$	$2H_0^2(m_\ell^2 - q^2)$	$-\frac{1}{2}(H_+^2 + H_-^2)(m_\ell^2 - q^2)$
$I_3^{a_1}$	$2H_+H_-(m_\ell^2 - q^2)$	$-H_+H_-(m_\ell^2 - q^2)$
$I_4^{a_1}$	$H_0(H_+ + H_-)(m_\ell^2 - q^2)$	$-\frac{1}{2}H_0(H_+ + H_-)(m_\ell^2 - q^2)$
$I_5^{a_1}$	$-2H_t(H_+ + H_-)m_\ell^2 - 2H_0(H_+ - H_-)q^2$	$H_t(H_+ + H_-)m_\ell^2 + H_0(H_+ - H_-)q^2$
$I_{6s}^{a_1}$	$2(H_+^2 - H_-^2)q^2$	$-4H_t H_0 m_\ell^2 + (H_+^2 - H_-^2)q^2$
$I_{6c}^{a_1}$	$-8H_t H_0 m_\ell^2$	$2(H_+^2 - H_-^2)q^2$
$I_7^{a_1}$	0	0

TABLE VI. Angular coefficient functions for $\bar{B} \rightarrow a_1(\rho\pi)\ell^-\bar{\nu}_\ell$: NP term with S operator, interference SM-NP with S operator, and NP-NP interference with S and T operators, Eq. (9).

i	$I_{i, }^{\text{NP},S}$	$I_{i, }^{\text{INT},S}$	$I_{i, }^{\text{INT},ST}$
$I_{1s}^{a_1}$	0	0	0
$I_{1c}^{a_1}$	$4H_t^2 \frac{q^4}{(m_b-m_u)^2}$	$4H_t^2 \frac{m_\ell q^2}{m_b-m_u}$	0
$I_{2s}^{a_1}$	0	0	0
$I_{2c}^{a_1}$	0	0	0
$I_3^{a_1}$	0	0	0
$I_4^{a_1}$	0	0	0
$I_5^{a_1}$	0	$-H_t(H_+ + H_-) \frac{m_\ell q^2}{m_b-m_u}$	$-2H_t(H_+^{\text{NP}} + H_-^{\text{NP}}) \frac{(q^2)^{3/2}}{m_b-m_u}$
$I_{6s}^{a_1}$	0	0	0
$I_{6c}^{a_1}$	0	$-4H_t H_0 \frac{m_\ell q^2}{m_b-m_u}$	$-H_t H_L^{\text{NP}} \frac{(q^2)^{3/2}}{m_b-m_u}$
$I_7^{a_1}$	0	$-H_t(H_+ - H_-) \frac{m_\ell q^2}{m_b-m_u}$	$-2H_t(H_+^{\text{NP}} - H_-^{\text{NP}}) \frac{(q^2)^{3/2}}{m_b-m_u}$

 TABLE VII. Angular coefficient functions for $\bar{B} \rightarrow a_1(\rho\pi)\ell^-\bar{\nu}_\ell$: NP term with S operator, interference SM-NP with S operator, and NP-NP interference with S and T operators, Eq. (9).

i	$I_{i,\perp}^{\text{NP},S}$	$I_{i,\perp}^{\text{INT},S}$	$I_{i,\perp}^{\text{INT},ST}$
$I_{1s}^{a_1}$	$2H_t^2 \frac{q^4}{(m_b-m_u)^2}$	$2H_t^2 \frac{m_\ell q^2}{m_b-m_u}$	0
$I_{1c}^{a_1}$	0	0	0
$I_{2s}^{a_1}$	0	0	0
$I_{2c}^{a_1}$	0	0	0
$I_3^{a_1}$	0	0	0
$I_4^{a_1}$	0	0	0
$I_5^{a_1}$	0	$\frac{1}{2}H_t(H_+ + H_-) \frac{m_\ell q^2}{m_b-m_u}$	$H_t(H_+^{\text{NP}} + H_-^{\text{NP}}) \frac{(q^2)^{3/2}}{m_b-m_u}$
$I_{6s}^{a_1}$	0	$-2H_t H_0 \frac{m_\ell q^2}{m_b-m_u}$	$-H_t H_L^{\text{NP}} \frac{(q^2)^{3/2}}{2(m_b-m_u)}$
$I_{6c}^{a_1}$	0	0	0
$I_7^{a_1}$	0	$\frac{1}{2}H_t(H_+ - H_-) \frac{m_\ell q^2}{m_b-m_u}$	$H_t(H_+^{\text{NP}} - H_-^{\text{NP}}) \frac{(q^2)^{3/2}}{m_b-m_u}$

 TABLE VIII. Angular coefficient functions for $\bar{B} \rightarrow a_1(\rho\pi)\ell^-\bar{\nu}_\ell$: NP term with T operator and interference SM-NP with T operator.

i	$I_{i, }^{\text{NP},T}$	$I_{i, }^{\text{INT},T}$
$I_{1s}^{a_1}$	$2[(H_+^{\text{NP}})^2 + (H_-^{\text{NP}})^2](3m_\ell^2 + q^2)$	$4(H_+^{\text{NP}}H_+ + H_-^{\text{NP}}H_-)m_\ell\sqrt{q^2}$
$I_{1c}^{a_1}$	$\frac{1}{8}(H_L^{\text{NP}})^2(m_\ell^2 + q^2)$	$H_L^{\text{NP}}H_0m_\ell\sqrt{q^2}$
$I_{2s}^{a_1}$	$2[(H_+^{\text{NP}})^2 + (H_-^{\text{NP}})^2](m_\ell^2 - q^2)$	0
$I_{2c}^{a_1}$	$-\frac{1}{8}(H_L^{\text{NP}})^2(m_\ell^2 - q^2)$	0
$I_3^{a_1}$	$-8H_+^{\text{NP}}H_-^{\text{NP}}(m_\ell^2 - q^2)$	0
$I_4^{a_1}$	$-\frac{1}{2}H_L^{\text{NP}}(H_+^{\text{NP}} + H_-^{\text{NP}})(m_\ell^2 - q^2)$	0
$I_5^{a_1}$	$-H_L^{\text{NP}}(H_+^{\text{NP}} - H_-^{\text{NP}})m_\ell^2$	$-\frac{1}{4}[H_L^{\text{NP}}(H_+ - H_-) + 8H_+^{\text{NP}}(H_t + H_0) + 8H_-^{\text{NP}}(H_t - H_0)]m_\ell\sqrt{q^2}$
$I_{6s}^{a_1}$	$8[(H_+^{\text{NP}})^2 - (H_-^{\text{NP}})^2]m_\ell^2$	$4(H_+^{\text{NP}}H_+ - H_-^{\text{NP}}H_-)m_\ell\sqrt{q^2}$
$I_{6c}^{a_1}$	0	$-H_L^{\text{NP}}H_t m_\ell\sqrt{q^2}$
$I_7^{a_1}$	0	$-\frac{1}{4}[H_L^{\text{NP}}(H_+ + H_-) - 8H_+^{\text{NP}}(H_t + H_0) + 8H_-^{\text{NP}}(H_t - H_0)]m_\ell\sqrt{q^2}$

TABLE IX. Angular coefficient functions for $\bar{B} \rightarrow a_1(\rho\pi)\ell^-\bar{\nu}_\ell$: NP term with T operator and interference SM-NP with T operator, Eq. (9).

i	$I_{i,\perp}^{\text{NP},T}$	$I_{i,\perp}^{\text{INT},T}$
$I_{1s}^{a_1}$	$[(H_+^{\text{NP}})^2 + (H_-^{\text{NP}})^2](3m_\ell^2 + q^2) + \frac{1}{16}(H_L^{\text{NP}})^2(m_\ell^2 + q^2)$	$\frac{1}{2}[4(H_+^{\text{NP}}H_+ + H_-^{\text{NP}}H_-) + H_L^{\text{NP}}H_0]m_\ell\sqrt{q^2}$
$I_{1c}^{a_1}$	$2[(H_+^{\text{NP}})^2 + (H_-^{\text{NP}})^2](3m_\ell^2 + q^2)$	$4(H_+^{\text{NP}}H_+ + H_-^{\text{NP}}H_-)m_\ell\sqrt{q^2}$
$I_{2s}^{a_1}$	$[(H_+^{\text{NP}})^2 + (H_-^{\text{NP}})^2](m_\ell^2 - q^2) - \frac{1}{16}(H_L^{\text{NP}})^2(m_\ell^2 - q^2)$	0
$I_{2c}^{a_1}$	$2[(H_+^{\text{NP}})^2 + (H_-^{\text{NP}})^2](m_\ell^2 - q^2)$	0
$I_3^{a_1}$	$4H_+^{\text{NP}}H_-^{\text{NP}}(m_\ell^2 - q^2)$	0
$I_4^{a_1}$	$\frac{1}{4}H_L^{\text{NP}}(H_+^{\text{NP}} + H_-^{\text{NP}})(m_\ell^2 - q^2)$	0
$I_5^{a_1}$	$\frac{1}{2}H_L^{\text{NP}}(H_+^{\text{NP}} - H_-^{\text{NP}})m_\ell^2$	$\frac{1}{8}[H_L^{\text{NP}}(H_+ - H_-) + 8H_+^{\text{NP}}(H_t + H_0) + 8H_-^{\text{NP}}(H_t - H_0)]m_\ell\sqrt{q^2}$
$I_{6s}^{a_1}$	$4[(H_+^{\text{NP}})^2 - (H_-^{\text{NP}})^2]m_\ell^2$	$-\frac{1}{2}[-4(H_+^{\text{NP}}H_+ - H_-^{\text{NP}}H_-) + H_L^{\text{NP}}H_t]m_\ell\sqrt{q^2}$
$I_{6c}^{a_1}$	$8[(H_+^{\text{NP}})^2 - (H_-^{\text{NP}})^2]m_\ell^2$	$4(H_+^{\text{NP}}H_+ - H_-^{\text{NP}}H_-)m_\ell\sqrt{q^2}$
$I_7^{a_1}$	0	$\frac{1}{8}[H_L^{\text{NP}}(H_+ + H_-) - 8H_+^{\text{NP}}(H_t + H_0) + 8H_-^{\text{NP}}(H_t - H_0)]$

TABLE X. $B \rightarrow \pi$ form factor parameters in Eq. (C1).

	$f_+^{B \rightarrow \pi}$	$f_0^{B \rightarrow \pi}$	$f_T^{B \rightarrow \pi}$
a_0	0.416(20)	0.492(20)	0.400(21)
a_1	-0.430	-1.35	-0.50
a_2	0.114	2.50	0.00076
a_3			0.534

$$f_{+,T}(t) = \frac{1}{1 - \frac{q^2}{m_{\text{pole}}^2}} \sum_{n=0}^{N-1} a_n [z(t)^n - \frac{n}{N} (-1)^{n-N} z(t)^N]$$

$$f_0(t) = \sum_{n=0}^{N-1} a_n z(t)^n, \quad (\text{C1})$$

expressed as a truncated series in the variable

$$z(t) = \frac{\sqrt{t_+ - t} - \sqrt{t_+ - t_0}}{\sqrt{t_+ - t} + \sqrt{t_+ - t_0}}. \quad (\text{C2})$$

In this expression, $t_+ = (m_B + m_\pi)^2$, and t_0 is chosen at the value $t_0 = (m_B + m_\pi)(\sqrt{m_B} - \sqrt{m_\pi})^2$. For $\bar{B} \rightarrow \pi\mu^-\bar{\nu}_\mu$, the kinematic range is $-0.279 \leq z \leq 0.283$; for $\bar{B} \rightarrow \pi\tau^-\bar{\nu}_\tau$, it is $-0.279 \leq z \leq 0.257$. The mass of the pole in $f_{+,T}$ is $m_{\text{pole}} = m_{B^*}$. The parameters a_n for f_+, f_0 , and f_T , with the condition $f_+(0) = f_0(0)$, are obtained by fitting the light-cone QCD sum rule results in the range $m_\ell^2 \leq q^2 \leq 12 \text{ GeV}^2$ [62,63] and the lattice QCD results for $16 \text{ GeV}^2 \leq q^2$ in the recent FLAG report [64]: they are in Table X. The other parameters used in the analysis are the quark masses $m_u = 2.16_{-0.26}^{+0.49} \text{ MeV}$ (in the $\overline{\text{MS}}$ scheme at $\mu = 2 \text{ GeV}$), $\bar{m}_b(\bar{m}_b) = 4.18_{-0.03}^{+0.04} \text{ GeV}$ [59], and the B decay constant $f_B = 188 \pm 7 \text{ MeV}$ [64].

- [1] J. P. Lees *et al.* (BABAR Collaboration), *Phys. Rev. Lett.* **109**, 101802 (2012).
[2] J. P. Lees *et al.* (BABAR Collaboration), *Phys. Rev. D* **88**, 072012 (2013).

- [3] M. Huschle *et al.* (Belle Collaboration), *Phys. Rev. D* **92**, 072014 (2015).
[4] Y. Sato *et al.* (Belle Collaboration), *Phys. Rev. D* **94**, 072007 (2016).

- [5] S. Hirose *et al.* (Belle Collaboration), *Phys. Rev. Lett.* **118**, 211801 (2017).
- [6] S. Hirose *et al.* (Belle Collaboration), *Phys. Rev. D* **97**, 012004 (2018).
- [7] R. Aaij *et al.* (LHCb Collaboration), *Phys. Rev. Lett.* **115**, 111803 (2015); **115**, 159901(E) (2015).
- [8] R. Aaij *et al.* (LHCb Collaboration), *Phys. Rev. D* **97**, 072013 (2018).
- [9] R. Aaij *et al.* (LHCb Collaboration), *Phys. Rev. Lett.* **120**, 171802 (2018).
- [10] A. Abdesselam *et al.* (Belle Collaboration), arXiv: 1904.08794.
- [11] Y. Amhis *et al.* (HFLAV Collaboration), *Eur. Phys. J. C* **77**, 895 (2017).
- [12] S. Fajfer, J. F. Kamenik, and I. Nisandzic, *Phys. Rev. D* **85**, 094025 (2012).
- [13] P. Biancofiore, P. Colangelo, and F. De Fazio, *Phys. Rev. D* **87**, 074010 (2013).
- [14] R. Aaij *et al.* (LHCb Collaboration), *Phys. Rev. Lett.* **120**, 121801 (2018).
- [15] R. Dutta and A. Bhol, *Phys. Rev. D* **96**, 076001 (2017).
- [16] R. Watanabe, *Phys. Lett. B* **776**, 5 (2018).
- [17] C.-T. Tran, M. A. Ivanov, J. G. Krner, and P. Santorelli, *Phys. Rev. D* **97**, 054014 (2018).
- [18] R. Aaij *et al.* (LHCb Collaboration), *Phys. Rev. Lett.* **122**, 191801 (2019).
- [19] R. Aaij *et al.* (LHCb Collaboration), *J. High Energy Phys.* **08** (2017) 055.
- [20] A. Abdesselam *et al.* (Belle Collaboration), arXiv: 1904.02440.
- [21] S. Bifani, S. Descotes-Genon, A. R. Vidal, and M.-H. Schune, *J. Phys. G* **46**, 023001 (2019).
- [22] R. Aaij *et al.* (LHCb Collaboration), *Phys. Rev. Lett.* **111**, 191801 (2013).
- [23] R. Aaij *et al.* (LHCb Collaboration), *J. High Energy Phys.* **02** (2016) 104.
- [24] R. Aaij *et al.* (LHCb Collaboration), *J. High Energy Phys.* **09** (2015) 179.
- [25] J. P. Lees *et al.* (BABAR Collaboration), *Phys. Rev. Lett.* **123**, 091801 (2019).
- [26] E. Waheed *et al.* (Belle Collaboration), *Phys. Rev. D* **100**, 052007 (2019).
- [27] S. Jaiswal, S. Nandi, and S. K. Patra, *J. High Energy Phys.* **12** (2017) 060.
- [28] D. Bigi, P. Gambino, and S. Schacht, *Phys. Lett. B* **769**, 441 (2017).
- [29] B. Grinstein and A. Kobach, *Phys. Lett. B* **771**, 359 (2017).
- [30] P. Gambino, M. Jung, and S. Schacht, *Phys. Lett. B* **795**, 386 (2019).
- [31] P. Colangelo and F. De Fazio, *Phys. Rev. D* **95**, 011701 (2017).
- [32] P. Colangelo and F. De Fazio, *J. High Energy Phys.* **06** (2018) 082.
- [33] R. Alonso, A. Kobach, and J. Martin Camalich, *Phys. Rev. D* **94**, 094021 (2016).
- [34] D. Becirevic, S. Fajfer, I. Nisandzic, and A. Tayduganov, *Nucl. Phys.* **B946**, 114707 (2019).
- [35] Z. Ligeti, M. Papucci, and D. J. Robinson, *J. High Energy Phys.* **01** (2017) 083.
- [36] A. K. Alok, D. Kumar, S. Kumbhakar, and S. U. Sankar, *Phys. Rev. D* **95**, 115038 (2017).
- [37] C.-H. Chen and S.-h. Nam, *Phys. Lett. B* **666**, 462 (2008).
- [38] A. J. Buras, K. Gemmler, and G. Isidori, *Nucl. Phys.* **B843**, 107 (2011).
- [39] A. Crivellin, *Phys. Rev. D* **81**, 031301 (2010).
- [40] A. Crivellin and S. Pokorski, *Phys. Rev. Lett.* **114**, 011802 (2015).
- [41] F. U. Bernlochner, Z. Ligeti, and S. Turczyk, *Phys. Rev. D* **90**, 094003 (2014).
- [42] F. U. Bernlochner, *Phys. Rev. D* **92**, 115019 (2015).
- [43] M. Blanke, A. Crivellin, S. de Boer, M. Moscati, U. Nierste, I. Nisandzic, and T. Kitahara, *Phys. Rev. D* **99**, 075006 (2019).
- [44] M. Blanke, A. Crivellin, T. Kitahara, M. Moscati, U. Nierste, and I. Nisandzic, *Phys. Rev. D* **100**, 035035 (2019).
- [45] G. Banelli, R. Fleischer, R. Jaarsma, and G. Tetlalmatzi-Xolocotzi, *Eur. Phys. J. C* **78**, 911 (2018).
- [46] W. Buchmuller and D. Wyler, *Nucl. Phys.* **B268**, 621 (1986).
- [47] V. Cirigliano, J. Jenkins, and M. Gonzalez-Alonso, *Nucl. Phys.* **B830**, 95 (2010).
- [48] M. Jung and D. M. Straub, *J. High Energy Phys.* **01** (2019) 009.
- [49] A. Celis, M. Jung, X.-Q. Li, and A. Pich, *Phys. Lett. B* **771**, 168 (2017).
- [50] J. Charles, A. Le Yaouanc, L. Oliver, O. Pene, and J. C. Raynal, *Phys. Rev. D* **60**, 014001 (1999).
- [51] M. Beneke and T. Feldmann, *Nucl. Phys.* **B592**, 3 (2001).
- [52] C. F. Uhlemann and N. Kauer, *Nucl. Phys.* **B814**, 195 (2009).
- [53] C. L. Y. Lee, M. Lu, and M. B. Wise, *Phys. Rev. D* **46**, 5040 (1992).
- [54] S. Faller, T. Feldmann, A. Khodjamirian, T. Mannel, and D. van Dyk, *Phys. Rev. D* **89**, 014015 (2014).
- [55] X.-W. Kang, B. Kubis, C. Hanhart, and U.-G. Meiner, *Phys. Rev. D* **89**, 053015 (2014).
- [56] C. Hambrock and A. Khodjamirian, *Nucl. Phys.* **B905**, 373 (2016).
- [57] S. Cheng, A. Khodjamirian, and J. Virto, *J. High Energy Phys.* **05** (2017) 157.
- [58] S. Cheng, A. Khodjamirian, and J. Virto, *Phys. Rev. D* **96**, 051901 (2017).
- [59] M. Tanabashi *et al.* (Particle Data Group), *Phys. Rev. D* **98**, 030001 (2018).
- [60] A. Sibidanov *et al.* (Belle Collaboration), *Phys. Rev. Lett.* **121**, 031801 (2018).
- [61] P. Hamer *et al.* (Belle Collaboration), *Phys. Rev. D* **93**, 032007 (2016).
- [62] I. S. Imson, A. Khodjamirian, T. Mannel, and D. van Dyk, *J. High Energy Phys.* **02** (2015) 126.
- [63] A. Khodjamirian and A. V. Rusov, *J. High Energy Phys.* **08** (2017) 112.
- [64] S. Aoki *et al.* (Flavour Lattice Averaging Group), arXiv: 1902.08191.
- [65] A. Bharucha, D. M. Straub, and R. Zwicky, *J. High Energy Phys.* **08** (2016) 098.
- [66] P. Ball and R. Zwicky, *Phys. Rev. D* **71**, 014029 (2005).

- [67] D. Du, A. X. El-Khadra, S. Gottlieb, A. S. Kronfeld, J. Laiho, E. Lunghi, R. S. Van de Water, and R. Zhou, *Phys. Rev. D* **93**, 034005 (2016).
- [68] R. Dutta and A. Bhol, *Phys. Rev. D* **96**, 036012 (2017).
- [69] S. Sahoo, A. Ray, and R. Mohanta, *Phys. Rev. D* **96**, 115017 (2017).
- [70] C.-H. Chen and T. Nomura, *Phys. Rev. D* **98**, 095007 (2018).
- [71] C.-H. Chen and C.-Q. Geng, *J. High Energy Phys.* **10** (2006) 053.
- [72] B. Aubert *et al.* (BABAR Collaboration), *Phys. Rev. D* **81**, 052009 (2010).
- [73] J. Dalseno *et al.* (Belle Collaboration), *Phys. Rev. D* **86**, 092012 (2012).
- [74] A. J. Bevan *et al.* (BABAR and Belle Collaborations), *Eur. Phys. J. C* **74**, 3026 (2014).
- [75] D. Scora and N. Isgur, *Phys. Rev. D* **52**, 2783 (1995).
- [76] A. Deandrea, R. Gatto, G. Nardulli, and A. D. Polosa, *Phys. Rev. D* **59**, 074012 (1999).
- [77] T. M. Aliev and M. Savci, *Phys. Lett. B* **456**, 256 (1999).
- [78] H.-Y. Cheng, C.-K. Chua, and C.-W. Hwang, *Phys. Rev. D* **69**, 074025 (2004).
- [79] H.-Y. Cheng and K.-C. Yang, *Phys. Rev. D* **76**, 114020 (2007).
- [80] Z.-G. Wang, *Phys. Lett. B* **666**, 477 (2008).
- [81] K.-C. Yang, *Phys. Rev. D* **78**, 034018 (2008).
- [82] R.-H. Li, C.-D. Lu, and W. Wang, *Phys. Rev. D* **79**, 034014 (2009).
- [83] S. Momeni and R. Khosravi, *Phys. Rev. D* **96**, 016018 (2017).
- [84] X.-W. Kang, T. Luo, Y. Zhang, L.-Y. Dai, and C. Wang, *Eur. Phys. J. C* **78**, 909 (2018).
- [85] F. De Fazio, T. Feldmann, and T. Hurth, *Nucl. Phys.* **B733**, 1 (2006); **B800**, 405 (2008).
- [86] F. De Fazio, T. Feldmann, and T. Hurth, *J. High Energy Phys.* **02** (2008) 031.
- [87] A. Khodjamirian, T. Mannel, and N. Offen, *Phys. Rev. D* **75**, 054013 (2007).
- [88] C. Bourrely, I. Caprini, and L. Lellouch, *Phys. Rev. D* **79**, 013008 (2009); **82**, 099902(E) (2010).